DELFT UNIVERSITY OF TECHNOLOGY

MASTER THESIS

Retained austenite in silicon-containing bainitic spring steels for trucks

by

PAWAN RAJASHEKHARUNI

(4786963)

Supervisors:
Dr.ir. S.E Offerman (TU Delft)
Dr. Lie Zhao (VDL Weweler B.V)

Committee members:
Dr.ir. S.E Offerman (TU Delft)
Dr. Lie Zhao (VDL Weweler B.V)
Dr.ir. M.J.M. Hermans (TU Delft)
Pablo Garcia Chao (TU Delft)

A thesis submitted in partial fulfillment of the requirements for the degree of Master of Science

in

Materials Science and Engineering, TU Delft

Acknowledgements

Firstly, I would like to thank my supervisors Dr.ir. S.E. Offerman and Dr. Lie Zhao, for giving me an opportunity to work on the current research which helped me in gaining an in-depth knowledge during the work days. The discussions and suggestions with them has driven me in the right path to achieve my goals. I would like to appreciate the support provided by them during the challenging times of COVID pandemic.

I would also like to thank Sander van Asperen and Richard Huizinga for helping during my experiments. I would like to specially thank Nico Geerlofs for conducting magnetisation measurements. Special thanks to Ph.D candidates Alfonso Navarro Lopez and Sudhindra Ayenampudi for sharing their knowledge. These talks helped me to the maximum extent during my thesis.

Last but not the least, I would like to take this opportunity to express my immense gratitude to my family (R. Sreenivasa Murthy, R. Lalitha and R.V.N. Kishore) for their unconditional support. I would also like to thank my friends for being my constant support which helped me in handling the toughest situations during my two years of life in The Netherlands.

2 years! 2 long years. Studying in TU Delft has not only provided me with acquiring scientific knowledge, but also taught me how to live. End to a magnificent part of the journey.

DELFT UNIVERSITY OF TECHNOLOGY

Abstract

Materials Science and Engineering, TU Delft

Master of Science

Retained austenite in silicon-containing bainitic spring steels for trucks

by P.N.K.Rajashekharuni

Bainitic steels are the type of steels which are widely in use, especially in automotive industries, for its good mechanical behaviour, i.e., with coexistence of strength, ductility and fatigue resistance. A better understanding on the mechanism and transformation kinetics of bainite are necessary in order to improve the performance of the bainitic steel further. This research mainly studies the kinetics of bainitic transformation during isothermal treatments. The chemical composition, in particular silicon (Si), affects the transformation kinetics of bainite, and therefore the fractions of retained austenite and bainitic ferrite.

The current research focuses on the bainite transformation kinetics during isothermal heat treatment. Steel specimens are austempered at 250°C, 300°C and 350°C and held for 30, 60 and 120 minutes, respectively. The steel in the current research has the alloy composition of Fe-0.61C-1.62Si-0.85Mn-0.32Cr (wt.%). Microstructures observed using optical micrographs consist of bainite and retained austenite after the austempering process. Quantitative measurements of the retained austenite (RA) fraction are performed by magnetisation technique. The results show that, at austempering temperatures of 250°C and 300°C, the fraction of retained austenite decreases gradually with increasing holding times and increases with increasing austempering temperatures. However, a different affect is observed in the steel austempered at 350°C for 30 minutes. The fraction of retained austenite increases from 30 to 60 minutes and subsequently decreases from 60 to 120 minutes. In order to study the effect of retained austenite on hardness resulting in decrease in overall hardness with increasing austempering temperatures and increases with increasing hold duration.

The JMAK model has been fitted to the observed fraction of austenite as function of time and temperature, which results in the parameters such as the rate constant and Avrami exponent. The fitted results suggest a one-dimensional grain growth of the bainite in this steel. The predictions from a thermodynamic analysis using the para-equilibrium model and the T_0-temperature are compared to the experimentally observed fractions of RA, which results in obtaining higher fractions than obtained experimentally. This thermodynamic analysis predicts an increase in the fraction of remaining austenite with increasing austempering temperature as observed experimentally in most cases. The thermodynamic study on the effect of Si concentration (1.62 wt.%) results shows that there is insufficient Si present in the steel to hinder the formation of cementite.

Keywords: Austempering, Bainitic ferrite, Retained austenite, Magnetisation technique, Mechanical properties, Kinetics of bainitic transformation, JMAK model, Para-equilibrium

Contents

List of Figures

List of Tables

List of Abbreviations

SEM	Scanning Electron Microscope
TTT	Time-transformation-temperature
M_s	Martensite start temperature
B_s	Bainite start temperature
$wt.\%$	Weight percentage
RA	Retained austenite
V_e	Extended volume
V	Total volume
V^α	Volume of α phase
dV_e^α	Excluded volume
G	Rate of growth of precipitates
τ	Particle nucleated time
I_v	Nucleation rate per unit volume
f	fraction of phase transformed
k_A, n	Avrami constants
$\Delta G_{\mathbf{f}}$	Gibbs free energy of bainitic ferrite
$\Delta G_{\mathbf{a}}$	Gibbs free energy of austenite
^oC	Degree Celsius
MA	Martensite-Retained austenite
f^α	Fraction of bainitic ferrite
f^γ	Fraction of retained austenite
$\chi^\gamma_{C_{350}}$	Carbon present in austenite at 350^oC
$\chi^\gamma_{C_{300}}$	Carbon present in austenite at 300^oC
f^B_{350}	Fraction of bainite formed at 350^oC
f^B_{300}	Fraction of bainite formed at 300^oC

Chapter 1

Introduction

1.1 Overview

This chapter begins with explaining the importance of the automotive steels that are used in heavy vehicle applications. A detailed description on the spring steels which is the area interest of the current research is discussed. Along with the importance of spring steel, the metallurgical aspects of the spring steel are also discussed using discrete sources.

1.2 Introduction to spring steels

Over several years, there have been tremendous amount of efforts made to develop the performance of the spring steel. In order to preserve the natural resources and maintain remunerative economic basis of fuel consumption and weight reduction of vehicles has become the recent trends in the automotive industries [1]. Weight reduction is one of the most important parameter is to maintain the sustainability of fuel consumption. This can be improved by understanding the microstructural evolution of the steels at various conditions.

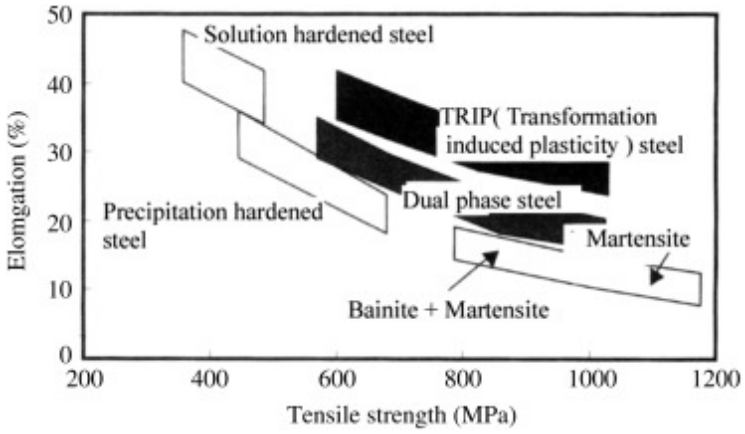

FIGURE 1.1: Evolution of steels with respect to their mechanical properties [2]

Automobiles are made of various types of steels with better formability to meet design requirements, corrosion resistance and impact resistance. Steels are one of the most prominent and popular materials due to the wide spread of its applications. Advanced high strength steel (AHSS) is a family of steels in automotive industry with good combination of strength and ductility [2]. AHSS consists of multiple phases present in the microstructures with chemical composition and precisely controlled cooling processes. Among all of AHSS, high-strength transformation-induced plasticity (TRIP) steel were considered over other steels (as shown in the figure 1.1). Considering the microstructural features by studying phase transformations, especially in TRIP and bainite

+ martensite steels, plays an important role in the development of the AHSS [2]. The main reason to consider phase transformations in bainitic and martensitic steels is because these steels show better strength when compared with other alternative phases such as ferrite, pearlite and austenite.

Among the family of AHSS, steels that are used for heavy load -carrying vehicles, consisting of spring steels are the current area of interest of the research. They are industrially produced with composition similar to medium carbon steels. Spring steels, also known as leaf spring is a kind of steel mainly used for suspension in the heavy vehicles. Spring steels are considered to be the most important component of the suspension system of heavy vehicles. They consist of a number of layers on top of one another with a gradual increase in size, the bigger layer is placed on the top. Springs steels are connected to the frame, either at both ends or at one end. For the latter, the front end is attached to the frame while the other end is attached to a short swinging arm through a shackle [3]. The main function of spring steel is to comfort the passengers by reducing the vertical vibration caused by the non-uniformity of road geometry during the motion of the vehicle [3]. In considerable efforts to improve the properties of spring steels, industries are developing various new alloys to the material. In recent years, bainitic spring steels have become the hot topic in the steel manufacturing industries, especially for heavy vehicle machinery. The automotive industries produces and sells trailing arms and air suspension systems for trucks, buses and trailers. The trailing arm is usually made of medium-carbon vanadium containing spring steels such as 51CrV4 steel. In order to replace expensive vanadium which is a critical raw material for the EU [4], high silicon spring steel such as 61SiCr7 is recently of great interest.

FIGURE 1.2: Trailing arm [5]

When a steel from an elevated temperature is quenched with higher cooling rate, the martensite is formed as an end microstructure. The quenched state of martensitic microstructure gives high mechanical properties such as strength and hardness, but not ductility. This is not suitable for heavy vehicle applications or even during manufacturing. Due to various heat treatment processes including tempering are performed to acquire desired mechanical properties. However, in comparison with properties and microstructure obtained by isothermal heat treatment i.e., bainite, are much tougher than the tempered martensite.

Among the alloying elements of the spring steel, the silicon content hinders the precipitation of cementite particles from the supersaturated ferrite and austenite. This mechanism leads to increment in the ductile property of the steel. A required amount of silicon can also promote the carbon partitioning into the residual austenite in the bainitic transformation. This results in the formation of large amount of retained austenite and martensite with high carbon content in the product microstructure. Therefore, study on the high silicon steels during the isothermal transformation plays an important role.

1.3 Metallurgical background of spring steel

1.3.1 Effect of alloying elements

The one of the most important aspect to understand the kinetics of bainitic transformation is to study the effect of alloying elements. During the manufacturing processes, the understanding of the kinetics during the isothermal heat treatment is also very important. There have been a lot of literature on the kinetics based on important parameters like chemical composition. The effect of alloying elements like silicon, manganese, carbon and chromium on the kinetics of isothermal treatments have been discussed in the literature.

Effect of silicon

The effect of silicon on the kinetics of bainitic formation during isothermal heat treatments has been discussed by various authors. Zener (1946), Ko and Cottrell and Bhadeshia [6, 7] stated that the bainitic ferrite is nucleated at the grain boundaries of austenite. They have also stated that the growth of the bainitic ferrite stops due to the instantaneous and displacive mechanism of the austenite. Subsequently, the carbon which is rejected from the supersaturated ferrite into the residual austenite in which carbides are formed with para-equilibrium composition. Y. Toji et al. [8] and T. Sourmail et al. [9] in their defense stated that the concentration of the silicon present in the steels has a decelerating effect on the kinetics of bainitic transformation. This is because large concentration of silicon content prevents the carbide precipitation,hence the carbon rejected by bainite enriches the austenite which is retained substantially stabilising the austenite. However, Karbakhsh Ravari et al. contradicted the results for hypo-eutectoid steels by describing that silicon can accelerate the kinetics of bainitic transformation, by reducing the amount of cementite during the bainitic transformation [10].

In literature, the time as a function of temperature plot in para-equilibrium condition, for analysing the precipitation in steel with high carbon content of 1.2% having varying silicon content has been studied by Kozeschnik and Bhadeshia [11]. The amount of silicon content in the figure 1.3 ranges from $1 - 2\%$. From the figure, it has been understood that it is difficult to hinder the precipitation of cementite at such low silicon concentrations. The impact of para-equilibrium on the cementite precipitation from parent austenite phase has also been discussed in Kozeschnik and Bhadeshia work. This is due to the entrapment of silicon in cementite, leading to reduction in free energy.

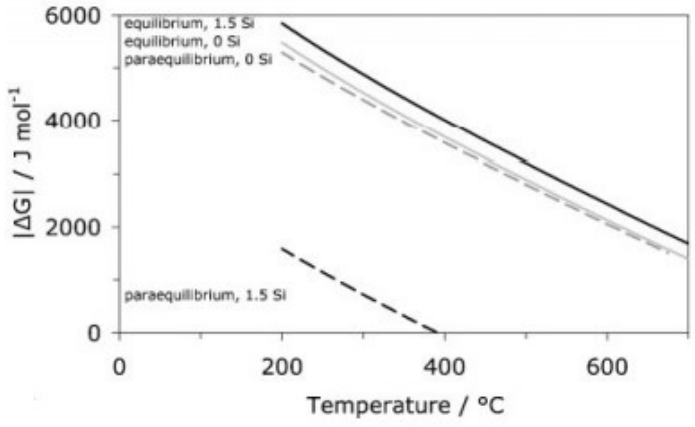

FIGURE 1.3: Free energy change for both equilibrium and para-equilibrium conditions as a function of silicon concentrations [11]

Changle Zhang and Hanguang Fu et al. [12] conducted an experiment on the steel containing more than 2% silicon concentration. It has been concluded that the steels with higher silicon concentration, decomposed austenite to a greater extent. Figure 1.4a states that RA gradually decreases with increasing silicon content during normalized process. From figure 1.4b, it has been also verified using micro-hardness measurements that when the steel with silicon concentration 2.5%, due to the decomposition of austenite to bainite containing bainitic ferrite acicular in nature resulting in the increment in hardness values.

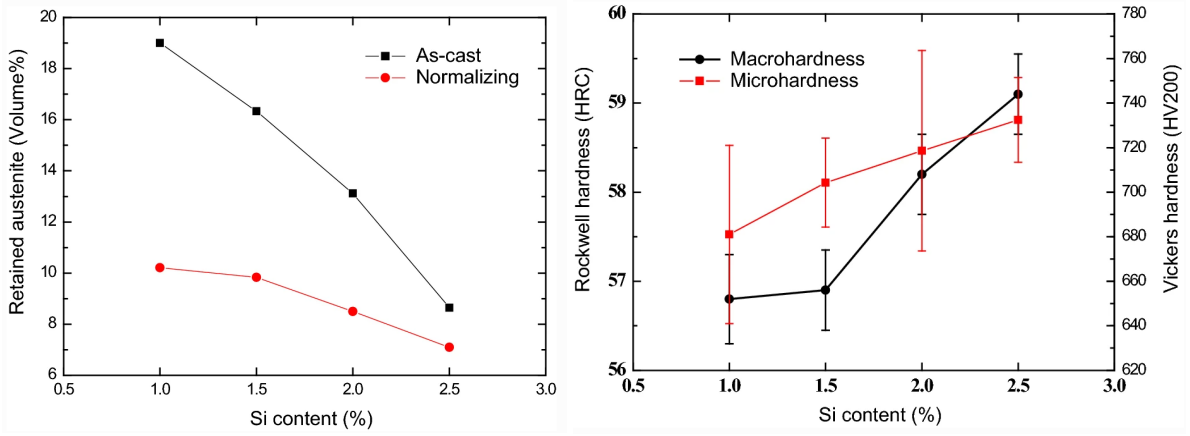

(A) (B)

FIGURE 1.4: (A) Effect of Si content on the retained austenite volume fraction and (B) Effect of Si content on the hardness of as-cast Mn containing bainitic steel [12]

Effect of manganese, carbon and chromium

Karbakhsh Ravari et al. [10] also discussed that the effect of manganese on microstructure, properties and kinetics of bainitic transformation and have a decelerating effect on the transformation kinetics of bainite during the isothermal treatments. Manganese in the austenite matrix acts as solid solution to increase the ferrite free energy and decrease that of austenite [13]. This delays the bainitic transformation and lowers the B_s temperature. Manganese shows improving tendency to mechanical properties such as strength, hardness and wear resistance in a bainitic steel. Manganese segregates at the austenite/austenite grain boundary and when there is more amount of manganese than required,it leads to enhancement in brittleness. As the amount of manganese increases within the limit, it affects the strength of the bainitic steel by increasing the retained austenite stability, where the film-like retained austenite increases in which bainitic ferritic laths are sub-divided into further finer laths so the strength of the steel increases gradually. The amount of manganese also increases the hardenability and reduces the driving force for bainitic transformation ata particular temperature and also stabilizes austenite [13]. The presence of silicon and manganese together enhances the bainitic transformation and distinguishes the transformation from pearlitic transformation. As discussed, the increase in the manganese content increases the free energy of the ferrite and deceases the austenite,leading to postponement of the bainitic transformation by reducing the B_s temperature. This results in the far separation with the pearlitic transformation.

Kangying Zhu et al. discussed about the effect of carbon content on the kinetics. By increasing the carbon concentration from 0.1 to 0.3 wt.%, it decelerates the kinetics at the isothermal temperatures [14]. The effect of carbon content reduces the driving force for nucleation and growth kinetic of the bainitic transformation [15, 16]. During bainitic transformation, carbon atoms diffuse from bainitic ferrite to austenite where the carbon remains in the solid solution, so that the untransformed austenite is enriched in carbon [13]. Therefore, the bainitic ferrite and carbon enriched austenite are formed together during the transformation. Higher carbon content reduces the transformation rate by slowing down the nucleation and growth.

Chromium is an important element of wear-resistant steel, which can interact with carbon in solid solution strengthening, increasing the strength of bainite, and improving the stability of austenite. Better hardenability is obtained in presence of chromium, manganese and carbon elements together and properties are more uniformly distributed in the thicker section of steels [13]. In spring steels, during isothermal heat treatment, the precipitation of carbides in the bainitic matrix takes place due to quenching. Different types of chromium carbides such as M_7C_3 and $M_{23}C_6$, with different thermal stabilities can be obtained depending on the temperature. The size, shape and fraction of these chromium carbides influence the mechanical properties of the material by increasing the creep strength and also leads to secondary hardening. And, hindering the carbide precipitation through the heat treatments is the goal of the industrial research [17].

1.4 Structure of the thesis

The report consists of different sections. Introduction (chapter 1), introducing the basic information on the bainitic spring steels and literature on the effect of alloying elements by various authors. Literature study (chapter 2) presents various literature research related to the current work for a clear insight. Experimental methods (chapter 3), explains the complete procedure in which the experiments were conducted in order to obtain the results. Results and Discussion (chapter 4) portraying the results from the experiments and characterization techniques along with a detailed discussion on the correlation of results that are obtained. And finally, the Conclusion Recommendations (chapter 5), which will summarize the report and the results obtained along with a list of recommendations for the future research on a similar topic.

Chapter 2

Literature study

2.1 Overview

This chapter deals with the various literature survey that has been conducted in order to understand the bainitic transformation and its morphology in steels. Following this, a detailed description on the mechanism of the bainitic formation based on several parameters such as TTT diagrams are discussed on the literature available. A detailed understanding of the thermodynamics and kinetic involved in the formation of bainite is also discussed in this chapter. The characterisation of bainite which is formed during isothermal heat treatments near the M_s temperature is also presented in the current literature. This chapter ends with the research objectives of the current research which are derived from the literature will be discussed.

2.2 Bainitic transformation in steels

2.2.1 Phase transformation diagram

Over several years ago, a tremendous study on isothermal transformation of austenite at temperatures above which the martensite is formed has been in a great research. Bainite is a microstructure which is the product of decomposition of austenite (γ) to ferrite (α), which can be denoted by $\gamma \rightarrow \alpha$ during the transformation from a higher temperatures in steel. To understand the importance and morphology of bainite, first understanding different phases present in an iron-carbon equilibrium diagram, as shown in the figure 2.1, is imperative. Iron-carbon phase diagram elucidates various phase transformations at different temperatures for different composition ranges. When different alloying elements are added to the composition of a particular steel, it changes the stability of the phases. There are discrete alloying elements categorised depending on the phase they stabilize. Elements such as N, Mn, Co, Ni and Mo are categorised as *austenite stabilizers* and elements like Al, Cr, Si and Nb are *ferrite stabilizers*. Carbon is an interstitial element where the solid solubility of carbon in austenite ($\sim$ 2%) is much higher than in the ferrite ($\sim$ 0.025%) due to octahedral interstitial sites in the face centered cubic (γ) crystalline structure are higher than in body centered cubic structure (α). The carbon obtained during the phase transformation ($\gamma \rightarrow \alpha$) precipitates as cementite (Fe_3C) particles because product phase can not accommodate carbon.

Phase transformations are classified into three different types, firstly, diffusion dependent transformation where composition or the number of phases present in the material remains same, secondly, transformation dependent on diffusion in which composition of the phases are changed and thirdly, the diffusion-less transformation [18]. The kinetics of phase transformation generally occurs at two distinct stages: nucleation and grain growth.It can be understood that the phase transformation is not an instantaneous process, however, precipitation and growth of these large amount of tiny particles of the new phases takes place until the transformation is completed

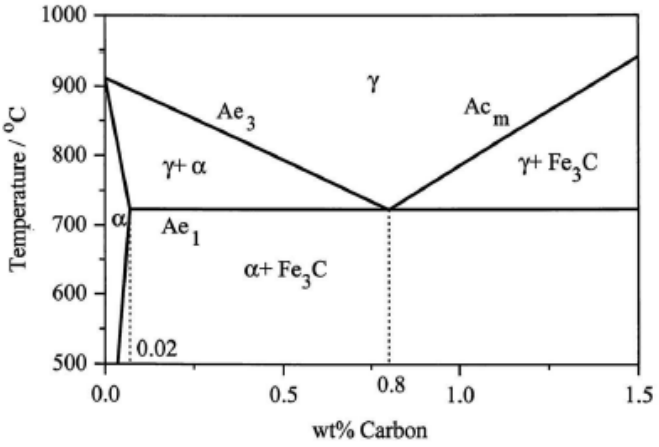

FIGURE 2.1: Iron-carbon equilibrium phase diagram

[18]. For a given composition, during the heat treatment processes, phase transformation occurs depending on the conditions. For example, when an alloy material is heated to the single-phase region i.e., to the austenitization temperature and subsequently cooled, the austenitic phase is decomposed into various other phases such as ferrite, pearlite, bainite and martensite depending on the heating and cooling rates. The microstructure formed during cooling determines the mechanical properties such as toughness and strength. Therefore, the study of phase transformations gives a better understanding to optimize the mechanical properties.

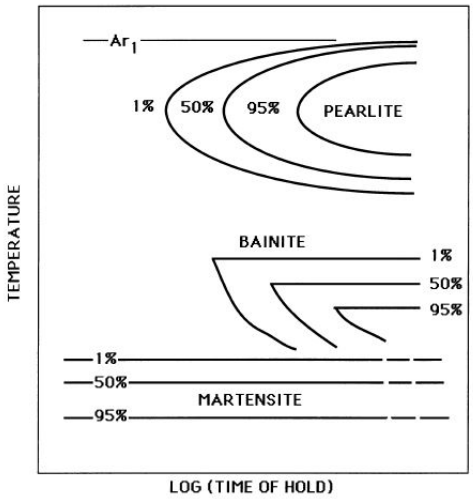

FIGURE 2.2: Schematic illustration of TTT diagram showing flat tops on the bainitic C-curves [19]

Fe-C diagram does not completely describes about the microstructural aspects after the transformation process. As the transformation in steels is time, temperature and composition dependent, time-temperature-transformation diagram plays an important role. Time-temperature-transformation diagram, also known as isothermal transformation diagram, gives the kinetics of the isothermal transformation. In steel alloys, austenite with face-centered cubic crystal structure is stable at higher temperatures, in which carbon occupies interstitial sites. When cooling the austenite at a certain rate, austenite will transform to other equilibrium phases at lower temperatures.The quantitative information of this transformation can be simply illustrated by

a time-temperature-transformation diagram (TTT diagram) which consists of several roughly C-shaped curves.The three C-curves at higher temperature range represent diffusional or reconstructive transformation products such as pearlite in the original austenite grain. The curves from left to right represent that 1%, 50% and 95% of the transformation is completed, respectively. As illustrated in the figure 2.2, the curves at lower temperature range undergoes displacive reactions and results in phases such as bainite and martensite. The resulting microstructures depending on both cooling rate and temperature to which the material is cooled to. When a steel is cooled to a intermediate temperature range, bainitic microstructure can be obtained which is shown by the curves lower than those of pearlite. With even fast cooling rate to room temperature range, austenite directly transforms to martensite, the process of which is called martensitic transformation represented by the curves at the lowest positions (figure 2.2).

2.3 Bainite morphology

Bainite is a microstructures which is formed during isothermal decomposition of austenite from an elevated temperature to a particular temperature range, between pearlitic region and martensitic region. he product of the transformation was first identified by Davenport and Bain [3] during the study on the transformation of austenite in eutectoid steel. he end phase of the transformation is the combination of ferrite and cementite in acicular nature.In later investigations, it has been understood that bainite with discrete morphology is easily identified in steels with different compositions and transformation temperatures as shown in the figure 2.4. Bainite morphology, depending on the temperature manifests two different phases such as upper and lower bainite. The difference between the two morphologies is the rate of precipitation of carbides from the supersaturated ferrite, depending on the temperatures as shown in the figure 2.3. At higher temperatures, carbon is subjected to mobility to diffuse away from the bainitic ferrite and thus precipitates around the *sub-unit* region. This results in the formation of upper bainite, which is defined as the stacking of bainitic ferritic sub-units with carbide precipitates in between them. At lower temperatures, carbon has low mobility to diffuse away from the bainitic ferrite and the excess carbon in the ferrite precipitates within the bainitic ferritic plates. This is due to non-availability of enough time for carbon to escape completely from ferrite. This results in lower bainite.

Bainite consists of ferritic plates with cementite particles present in between the plates, also austenite which is not transformed. As discussed, the individual plates of ferrite are known as sub-units and a group of ferritic sub-units are known as sheaves, nucleates at austenitic grain boundaries and expands towards the centre of the grain. As the isothermal transformation temperature decreases, the nucleation of ferritic sub-units also decreases so as their density. The sheaf formation mechanism and its growth also gives information on the rate of lengthening of the sheaf which is less than the individual sub-unit. It also depends on the time to which the growth of the sub-unit is saturated.

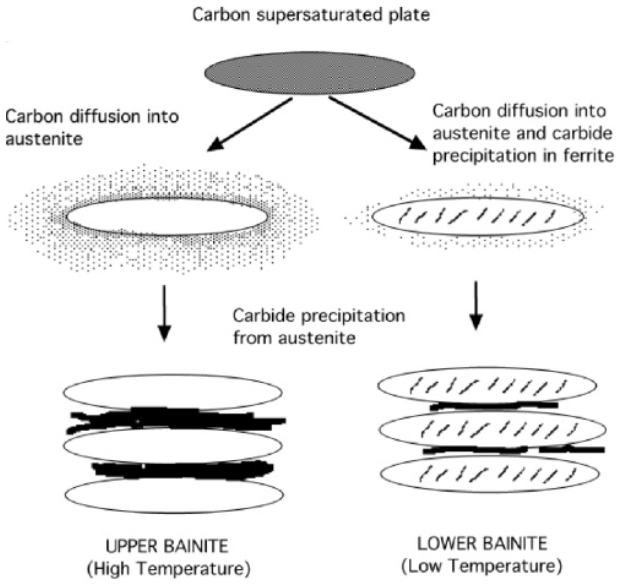

FIGURE 2.3: Schematic illustration of transition from upper to lower bainite [20]

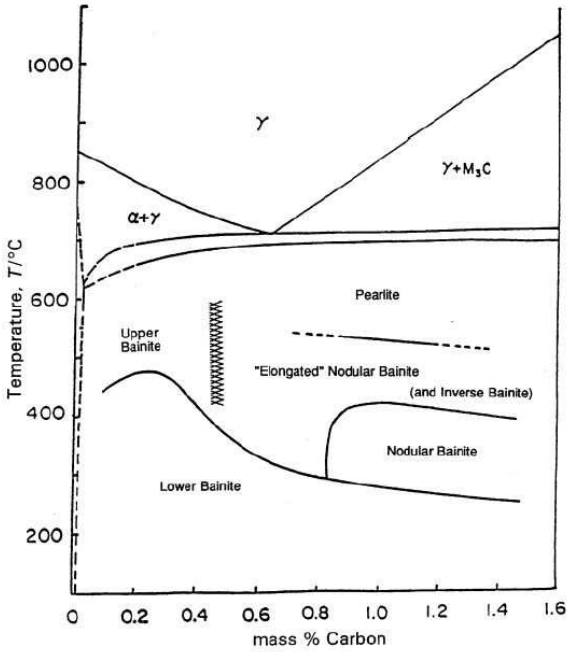

FIGURE 2.4: Schematic representation of different morphologies of bainite in various temperatures and compositions [21]

Upper bainite

Upper bainite consists of sheaves of ferritic sub-units with a similar orientation which are separated by cementite particles. In other words, it also depends on the carbon rejection rate from ferrite to austenite. Upper bainite forms at relatively high temperatures i.e., at the range of $350 - 500^0C$ [22]. Upper bainite as shown in the figure 2.5, where the nucleation of ferrite and carbon diffusion takes place in austenite matrix. As the temperature decreases, carbon undergoes

less diffusion and segregates along the grain boundaries of austenite as carbide precipitates.

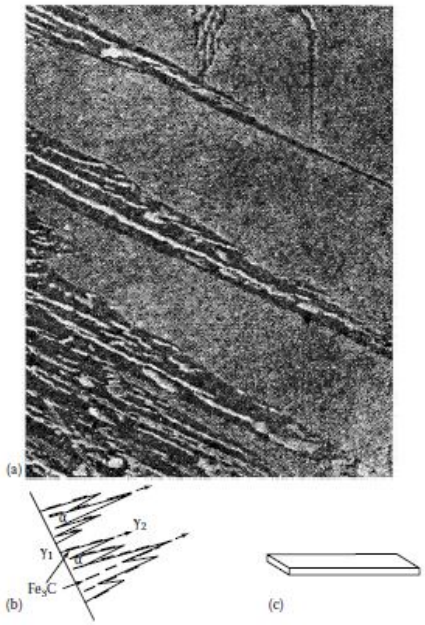

FIGURE 2.5: (a) Upper bainite in medium-carbon steel, (b) Schematic of growth mechanism and (c) Illustrating the shape of a 'lath' [22]

Lower bainite

As discussed previously, at a reduced transformation temperatures or when the amount of carbon concentration present is high, carbon precipitates in the intra-lath along with inter-lath regions of the sheaves of bainitic ferritic sub-units. The obtained microstructure is known as lower bainite. Lower bainite is generally formed at a range of $200 - 350^0C$ [22]. Whereas, as shown in the figure 2.6, the carbon present in the ferritic region is high due to less diffusivity of carbon taking place at lower temperatures, giving the carbide precipitates within the ferritic region. The carbides formed within the bainitic ferrite minimizes the free energy, due to the ferrite growth. The carbides inside a single ferrite plate of lower bainite usually are aligned along the same axis parallel to each other. Therefore, two types of cementite can be recognised in lower bainite: cementite particles that precipitated from the carbon enriched austenite and cementite particles that precipitated from supersaturated ferrite. The layers of carbide in lower bainite are usually extremely fine compared with those in upper bainite.

Consequently, steels with lower bainitic microstructure are tougher than the steels with upper bainitic microstructure. Moreover, lower bainite is stronger than upper bainite since the precipitates are finer.

2.3.1 Bainitic microstructures

In the previous section, the basic microstructures of upper and lower bainitic have been introduced. In this section, the bainitic microstructures obtained by isothermal heat treatment in a silicon steel will be discussed. As discussed, carbide precipitation can be hindered when there is a high amount of silicon present in the composition of the steel, which is around 1.5 - 2 wt.% [13].

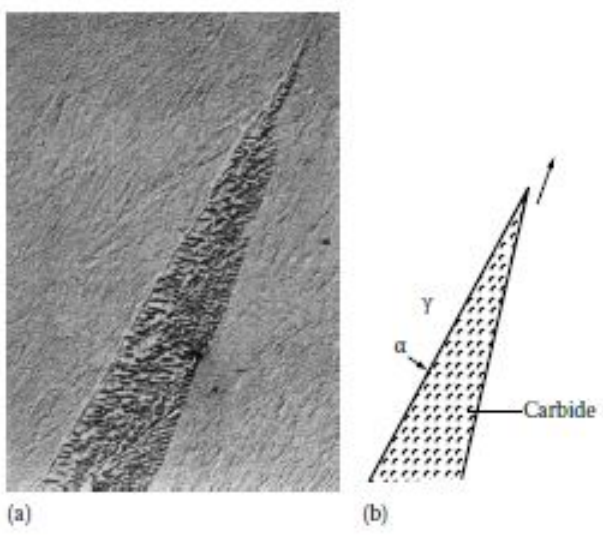

FIGURE 2.6: (a) Lower bainite in 0.69wt% C low-alloy steel (b) A possible growth mechanism, carbides precipitate at interface thereby removing the excess carbon in front of the . [22]

It is also possible to obtain retained austenite enriched with carbon during the transformation. The retained austenite is observed at bainitic ferritic laths and martensite-retained austenite (MA) blocks. These blocks of martensite and retained austenite are formed during the cooling process from relatively high temperatures to room temperature, where austenite is partially transformed to martensite, especially near grain boundaries. The retention of austenite during the transformation mainly contributes to the plasticity of the steel. Bainitic steels have good ductility due to retained austenite which can be formed in the inter-lath regions of ferritic laths. It can reduce the probability of initiation and propagation of cracks and contributes to TRIP effect. Figure 2.7 represents the bainitic microstructures of a Fe-0.51C-1.4Si-0.56Mn steel subjected to austempering at 290^oC and 330^oC for 60 min. The thicker sections of film-type retained austenite are observed in the micrograph representing the steel austempering 330^oC for 60 minutes, when compared with the steel austempered at 290^oC.

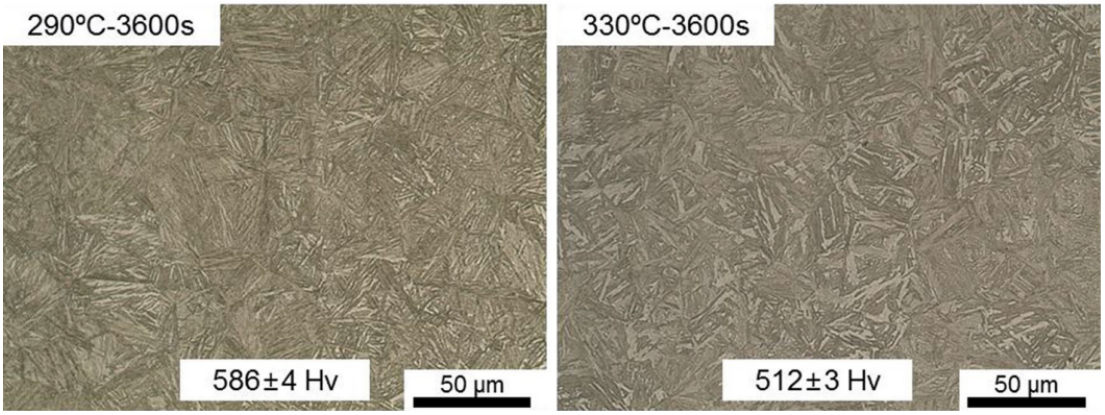

FIGURE 2.7: Optical micrographs at austempering conditions at 290^oC and 330^oC for 60 min [23]

2.4 Bainite formation mechanism

There are various kinetic models for bainite formation that have been widely in use in industry and research. Kinetics of bainitic transformation modeling is an underlying physical mechanism of the transformation. Thus, it is important to understand the fundamental aspects of mechanisms of the transformations. In these models, the consideration of the effect of carbide precipitation during bainitic transformation has been ruled out in high silicon bainitic steels, to avoid the interference of the cementite precipitation. Over a past few years, there are two theories of the kinetics of bainitic transformation, which are based on reconstructive and displacive mechanisms. Figure 2.8 is the schematic representation of the TTT diagram showing the upper and lower C-curves, which has a flat top at temperature T_h.

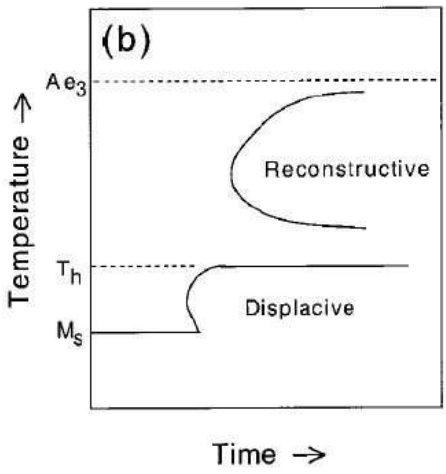

FIGURE 2.8: Schematic representation of C-curves with TTT diagram [24]

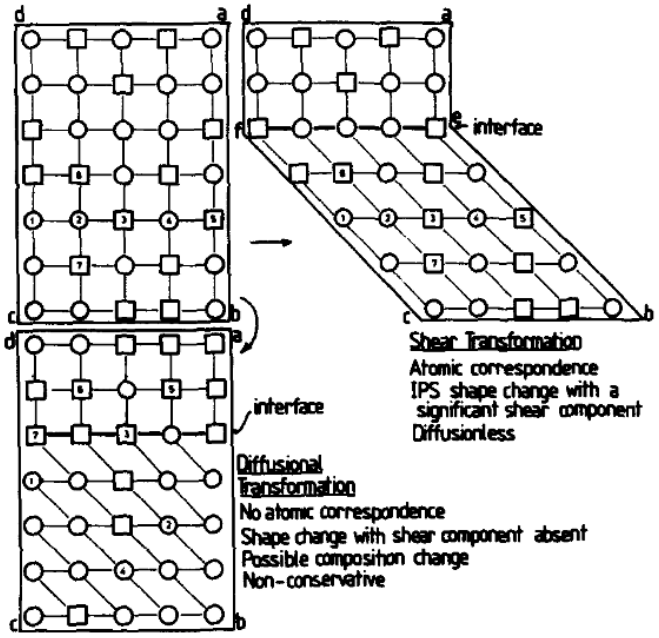

FIGURE 2.9: Schematic representation of the mechanisms of diffusional and displacive transformations [25]

The two mechanisms, reconstructive and displacive, describes different ways of rearrangement of the lattice atoms across the interface during the transformation. These two transformation mechanisms, that are schematically illustrated in the figure 2.9, will be discussed in detail in the following sections.

2.4.1 Reconstructive transformation mechanism

In reconstructive mechanism, all the atoms involves the diffusion at the interface during the transformation. This transformation process is a thermally activated process in which the change in the structure of the lattice by diffusion process resulting in minimizing the strain energy. in this transformation mechanism, there is also change in volume to a new structure. The end product of the diffusive mechanism results in allotriomorphic ferrite, idoimorphic ferrite and pearlite [25]. When the temperature is reduced from austenitizing temperature, ferrite and pearlite can coexist in equilibrium. As discussed, ferrite is present in the form of allotriomorphic initially. Idoimorphic ferrite is also formed by the same mechanism but the difference between both morphologies is that the ferrite is formed within the austenite grains. Pearlite formation takes place by the growth of both ferrite and cementite simultaneously. Pearlite is usually nucleates at grain boundaries or at the ferrite-austenite interface. Although both the phases grows cooperatively, the nucleation is imperatively depends on the alloy composition.

2.4.2 Displacive transformation mechanism

Displacive mechanism usually occurs at the lower temperatures. Atoms in this mechanism move in a synchronous manner and are displaced together across the interface. As this mechanism occurs at lower temperatures, there no influence of thermal activation that causes the transformation to take place with the diffusion of the substitutional atoms. This displacement of these atoms is less the inter-atomic spacing. Although, the chemical composition of the alloy remains same, there is a macroscopic change in the crystal structure. From figure 2.9, it has been understood that there is an atomic correspondence between the parent and product lattices. Therefore, in mechanisms like displacive, the transformation of substitutional atoms occurs without diffusion, where, the transformation of interstitial atoms may or may not diffuse, which does not affect the shape during the transformation.

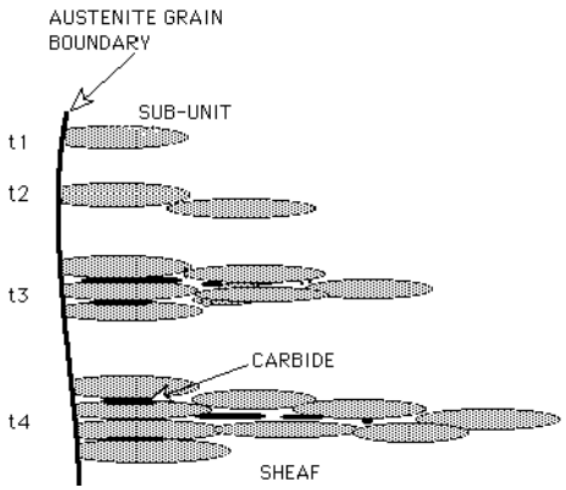

FIGURE 2.10: Sheaf formation of bainitic ferrite in displacing mechanism [26]

Surface relief which is caused due to the invariant plane strain is usually observed in the bainitic formation. At higher undercoolings of the steel, driving force for diffusion-less shear mechanism of the transformation takes places resulting in bainitic ferritic plates to nucleate at austenite grain boundaries. The growth of this *sub-unit* is hindered due to the dislocation present as a result of plastic deformation. Due to the available driving force, by *autocatalytic nucleation* playing an important role, allows the new *sub-units* to grow. Schematic representation of the growth of bainitic ferrite sub-units due to autocatalysis during the transformation is shown in the figure 2.10.

2.5 Austempering heat treatment

Austempering treatment, also known as isothermal heat-treatment process is applied when the steel is austenitised at a temperature above A_3 line and subsequently cooled to temperature below the pearlitic region and above M_s temperature and holding for several amount of time, the resultant microstructure is a mixture of bainite, martensite (after cooling to the room temperature) and retained austenite [27]. The figure 2.11 illustrates the TTT curve of Fe-0.55% C-1.62% Si-0.78% Mn-0.77% Cr medium carbon steel.

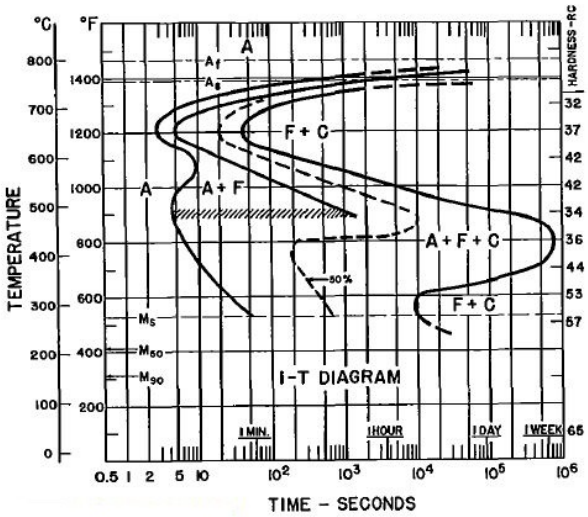

FIGURE 2.11: Schematic illustration of Time-transformation-temperature curve. The data corresponds to Fe-0.55% C-1.62% Si-0.78% Mn-0.77% Cr [28]

2.5.1 Decomposition of retained austenite

The role of retained austenite is very complex. Depending on its size, morphology and volume fraction distribution it influences the final engineering properties of the steel. Austenite remains untransformed upon rapid cooling even at the intermediate temperatures range. Inclusions like carbides can precipitate from retained austenite due to high diffusivity of carbon. In silicon-rich bainitic steels, as mentioned previously, large quantity of carbon enriched austenite is retained in MA blocks and as thin films among the bainitic sheaves. The austenite retained is present in two different morphologies such as block and thin-film forms. Thin films are observed between the sub-units of ferrite which contains high carbon concentration because of excess carbon diffusion from bainitic ferrite to austenite, whereas block form is observed in between the sheaves which are more thermally and mechanically stable. Kang et al. [29] investigated the isothermal heat treatments followed by tempering effect of bainitic steel (Fe-0.46C-1.55Si, wt.%) and microstructures shown in the figure 2.12.

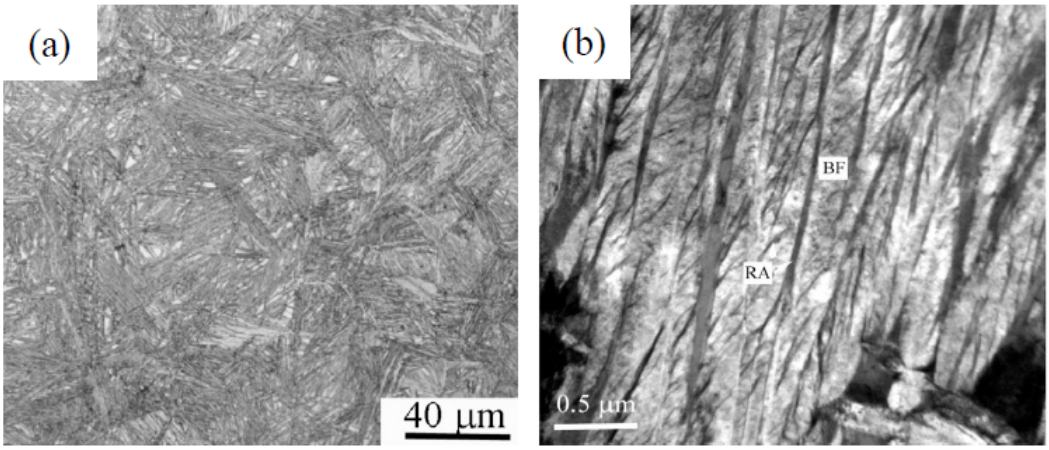

FIGURE 2.12: (a) Optical microscope microstructure (b) TEM microstructure of a medium carbon high silicon. The data corresponds to Fe-0.46% C-1.55% Si, isothermal transformed at 270^oC followed by tempering at 240^oC [29]

Several literature have been stated the decomposition of retained austenite using X-ray diffraction, quantitatively. Varshney et al. measured the fraction of RA of steel with 0.61C-1.71Si-0.86Mn composition with respect to isothermal holding times, as the function of austempering temperatures. It has been observed that RA fraction decreases with holding time [30]. A large difference in the amount of RA has been observed in the steel samples austempered at 300^oC and 400^oC, due to the large driving force for nucleation at lower temperatures. Similar observations have been observed in Liu et al. with 0.95C-2.90Si-0.75Mn-0.52Cr-0.25Mo steel composition which is austempered at a temperature range from 220^oC to 350^oC. During the heat treatment, less amount of RA is observed in the steel sample austempered at 220^oC [31].

2.5.2 Precipitation of carbides

It has been understood from the previous literature that cementite in upper bainite precipitates from the austenite matrix. The cementite precipitation reduces the stored energy at the interface region and even within the grains of ferrite, during the transformation. In lower bainite, it has been observed that precipitation of carbides initially takes place at the austenite-ferrite interface and from the austenite matrix and gradually incorporates into the ferrite plate [32]. Hehemann et al. stated that, on analysis of carbon content data of retained austenite it has been concluded that most of the carbides are precipitated from austenite [33].

The detailed investigation of the microstructures of lower bainite concluded that the ferritic plate nucleates and grows along the length from the grain edge with sidewise diffusion of carbon into the parent austenite, where initial sub-unit plates do not contain carbide precipitates [32]. The thickness of the edge of the plate gradually increases due to growth of ferrite and nucleation of carbides at the interface. Singh et al., stated that there is no clear information on the reason behind the degree of cooperation of formation of ferrite and carbides which is less in upper bainite [32].

2.6 Equilibrium near interface

In steels, the equilibrium near the interface of austenite and ferrite are defined by temperature and alloy composition. During the transformation under diffusion, the conditions near interface are identifiable. The diffusion controlled of moving interface of austenite and ferrite at a specific temperature is determined by phase diagram under equilibrium condition, as shown in the figure 2.13. In this figure, it can be understood that the concentration of ferrite and austenite for a specific steel and temperature, with carbon concentration in the bulk region. Under this condition, at the interface of ferrite and austenite phase contains equal chemical potential of *Fe* and *C*, leading to prevent the movement of interface.

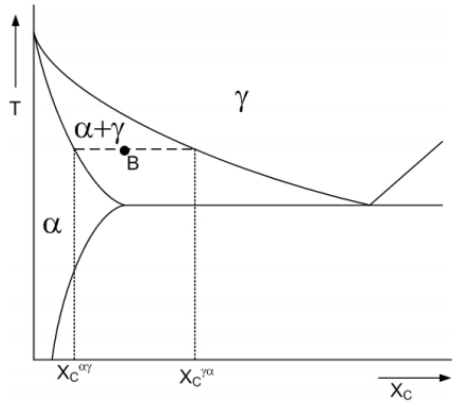

FIGURE 2.13: Schematic representation of the carbon concentration of ferrite and austenite under equilibrium condition, at a specific temperature [28]

In order to describe the equilibrium conditions near the interface, para-equilibrium condition is widely in use for bainitic steels. In this section, *'Para-equilibrium'* condition is explained.

2.6.1 Para-equilibrium

Para-equilibrium (PE) is defined as the kinetically constrained equilibrium of carbon near the interface and composition of the other substitutional elements remains the same. During the transformation, in PE condition, the substitutional atoms are not subjected to mobility across the interface. The conditions that are to be attained near the interface are, having same amount of alloying elements with respect to *Fe* on the both sides of the interface and having same chemical potential of carbon on either sides of the interface. For the figure 2.14, it can be observed that no concentration profile of substitutional alloying element is identified, however, carbon concentration profile in austenite is observed.

For instance, a substitutional alloying element M is partitioned among both the phases, α and γ at the interface. As mentioned in the previous paragraph, the chemical potential of carbon remains unchanged across the interface. This is expressed in equation 2.1.

$$\mu_C^{\alpha} = \mu_C^{\gamma} \tag{2.1}$$

The above equation gives the interface concentrations and also gives a better understanding of the kinetics of bainitic transformation in PE condition.

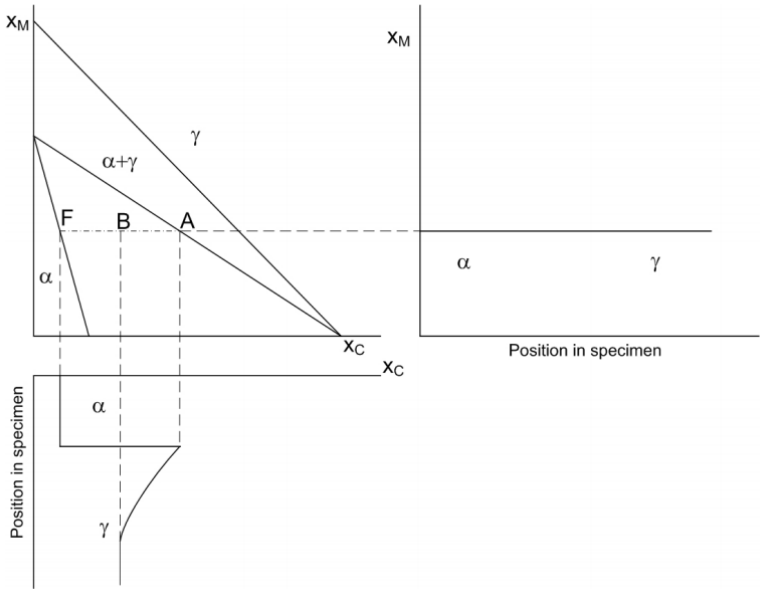

FIGURE 2.14: C and Mn concentration profiles in α and γ in a Fe-C-Mn system under PE condition [34]

2.7 Thermodynamics and kinetics of bainite

Zener assumed that the growth of bainite is a diffusion-less mechanism and during this growth, the excess carbon after supersaturation in bainitic ferrite is relieved and partitioned into residual austenite [19]. Figure 2.16 represents the free energy curves of austenite and ferrite at a specific temperature T_1 as function of carbon concentration. The intersection of these free energy curves describes, in a displacive mechanism, the carbon concentration above which γ cannot transform into α. When the intersection point is extrapolated, the carbon content as a function of temperature is termed as T_o curve. This states that, during isothermal heat treatment at T_1 if the precipitation of carbides does not takes place, the transformation will be terminated when the carbon concentration in austenite reaches T_o. However, during reconstructive mechanism, the carbon concentration in austenite is defined by Ae_3 and in ferrite it is defined by Ae_1, using the common tangent construction.

From figure 2.8, as the lower C-curve with the flat top edge representing displacive mechanism, it has been understood that the bainite-start and Widmanstatten ferrite start temperatures are difficult to distinguish. This condition is more sensitive to the steel composition, especially when transformation is conducted at that specific temperature (T_h). In displacive mechanism, at temperature T_h, it has established a *universal nucleation function* (G_N) because it is an important criterion which describes the driving force for nucleation of bainite and Widmanstatten ferrite.

During the transformation, nucleation involves diffusion of carbon [36]. At the same time, carbon must partition during the nucleation process for reduction in the free energy. However, it was found that diffusion-less nucleation is not feasible for carbon to partition because in certain conditions it may lead to increment in the free energy (ΔG_m). Figure 2.16 schematically represents the plot of chemical free energy change as a function of flat top temperature T_h where the displacive transformation occurs where every point in the plot represents discrete steels. On plotting the change in Gibbs free energy against flat temperature (T_h) for different steels, a linear relationship is derived. An empirical equation is obtained from the linear relationship, determining G_N which is expressed as:

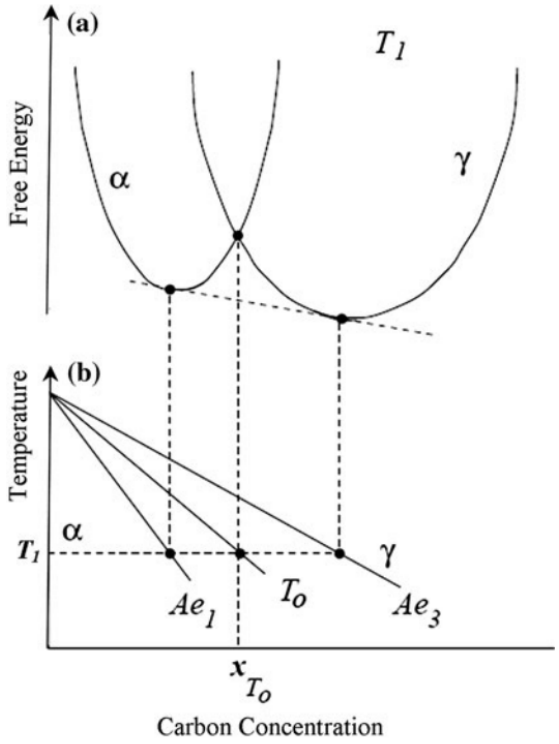

FIGURE 2.15: Schematic representation of free energy curves of austenite and ferrite at temperature T_1 [35]

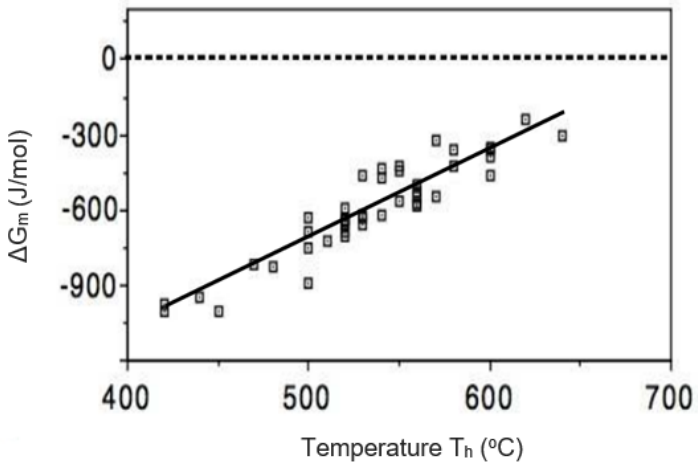

FIGURE 2.16: Change in free energy during nucleation plotted as a function of T_h representing partitioning of carbon in para-equilibrium condition [19]

$$G_N = C_1 T_h - C_2 J/mol \tag{2.2}$$

where, C_1 = 3.5463 J/mol K and C_2 = 3499.4 J/mol K [37]

Bainite is formed at specific temperatures in which the nucleation and growth conditions are satisfied in two forms.

- Firstly, the driving force for nucleation during the transformation must be greater than the general nucleation function. It is very difficult to find the difference between Widmanstatten ferrite and bainite morphology. In order to distinguish between the nucleus of Widmanstatten ferrite and of bainite at the flat top temperature T_h, the growth of these nuclei is an important parameter which differentiates both. This form is achieved when the following condition is satisfied:

$$\Delta G_m < G_N \tag{2.3}$$

  where, ΔG_m is the maximum free energy change available for nucleation in para-equilibrium condition at temperature T_h

- Secondly, the driving force for transformation from austenite to ferrite must exceed the bainite energy barrier. When the under-cooling is high in order to obtain bainite and by maintaining the driving force required for diffusion-less growth at the respective temperature, it is possible to distinguish the nucleus which is expected to be bainite, only the following condition has been satisfied:

$$\Delta G^{\gamma \rightarrow \alpha} < -G_B \tag{2.4}$$

  where, G_B is the stored energy of the bainite, with $400 J/mol$

2.7.1 Kinetics of bainitic transformation

As the bainitic transformation is a displacive mechanism, the isothermal transformation kinetics is controlled by the rate of nucleation mechanism and also depends on the atomic behaviour during the transformation. However, fraction of bainite formed during the transformation requires an understanding on impingement between the particles. The concept to understand the mechanism between the particles formed can be done by Johnson, Mehl, Avrami and Kolmogorov concept [19]. When two particles exists in a matrix, after a small time interval, during the transformation the previously existing particles grow and also new particle regions are formed.

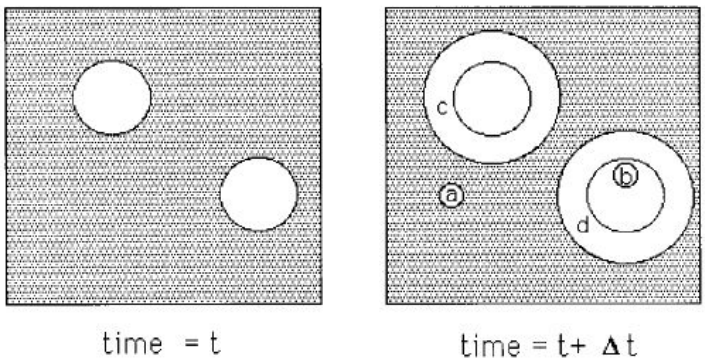

FIGURE 2.17: An illustration of the concept of extended volume. Two precipitate particles have nucleated together and grown to a finite size in the time t. New regions c and d are formed as the original particles grow, but a and b are new particles,of which b has formed in a region which is already transformed. [19]

However, due to the uncertainty, the change in the volume of the product phase can be calculated by [19]:

$$dV^{\alpha} = (1 - \frac{V^{\alpha}}{V})dV_e^{\alpha} \tag{2.5}$$

where, V_e is extended volume, V is the total volume, V^{α} is volume of α phase

In equation 2.5, to exclude the newly formed particles which are formed within the initial particles, which are not contributing to the product volume change, the change in excluded volume term (dV_e^{α}) is multiplied. When the newly formed precipitates are randomly distributed through out the matrix, to calculate the volume fraction of transformation, equation 2.5 can be integrated. Assuming the shape of the precipitates to be spherical and nucleation and growth of the precipitates are occurring at a rate of G, the change in extended volume over a time interval can be obtained by [19]:

$$dV_e^{\alpha} = \frac{4}{3}\pi G^3(t-\tau)^3 \times I_V \times V \times d\tau \tag{2.6}$$

where, τ is particle nucleated at time, I_V is the nucleation rate per unit volume

Now, substituting the equation 2.6 in equation 2.5, the real volume fraction can be calculated [19] ($f = V^{\alpha}/V$) by,

$$f = 1 - exp(-\pi G^3 I_v t^4/3) \tag{2.7}$$

A general form to derive the volume fraction under specific assumptions of a constant nucleation and growth rate and nucleation of particles randomly in a matrix where k_A and n are the function of time, temperature and other variables [19],

$$f = 1 - exp(-k_A t^n) \tag{2.8}$$

2.8 Research objectives

It is evident from the literature that it the acceleration or deceleration effect of alloying elements such as silicon on the transformation kinetics of bainite is not well understood. A study on effect of holding times during austempering temperatures could lead to a better understanding of the phenomenon and widen up the possibilities for the future. It is also necessary to conduction the necessary thermodynamic calculations which could support the experimental results for clear insight. According to the literature, the amount of retained austenite increases as with the isothermal temperature, whereas, the volume fraction of retained austenite decreases when the steel is subjected to longer holding time.

In various literature, there are quite a number of X-ray diffraction experiment that has been conducted to understand the effect of retained austenite on the kinetics of bainitic transformation. In current research, it is necessary to conduct magnetisation techniques which could help in comparison with the X-ray diffraction results of volume fraction of retained austenite for a better accuracy. Relating the microstructural properties with the mechanical properties will always gives better understanding of the concepts. A study on the effect of decarburized layer on the applications is also necessary. In order to study the microstructural evolution and effects of alloying elements on the kinetics of bainite, a medium carbon steel with composition, Fe-0.61C-1.62Si-0.85Mn-0.32Cr (wt%) has been used for the current research.

The key research question of the present work is:

- What is effect of retained austenite (RA) on the bainitic transformation of the silicon-containing bainitic spring steel?

In order to answer the research question, the present study will be focused on:

- To study the microstructural evolution of the steel subjected to isothermal heat-treatment at different austempering temperatures and holding times.
- Measuring the evolution of volume fraction of retained austenite present in the steel, as the function of different austempering temperatures and holding times.
- Understanding the mechanical properties of the steel by performing micro-hardness measurements.
- Performing calculations using a thermodynamic model which is represented as supporting information to analyze the effects of retained austenite obtained during isothermal treatment.

Chapter 3

Experimental methods

3.1 Overview

This chapter deals with the detailed experimental procedures conducted in this current research. The alloy composition used is introduced along with the selected theoretical properties of this alloy which are calculated alongside. An overview of the heat treatments performed in this work and the post-processing of the resulting samples is presented. Furthermore, the experimental details on the equipment used are also explained. Magnetisation, optical microscopy and micro-hardness measurements are extensively used to co-relate the results for obtaining better outcome which could be useful for the future applications.

3.2 Material

In order to study the evolution of microstructures during the austempering process, samples of steel alloy with iron, carbon, silicon, manganese and chromium are investigated. The samples with carbon content varying from 0.57 to 0.65 wt.%, manganese content varies from 0.70 to 1.0 wt.%, silicon content varying from 1.6 to 2.0 wt.% and while chromium content varies from 0.2 to 0.45 wt.% are heat-treated at different isothermal temperatures were considered for the investigation. The hypo-eutectoid 61SiCr7 steel samples were hot-rolled with a specific composition, is observed in Table 3.2. As shown from the figure 3.1, the samples were considered 15cm away from the ring end of the spring steel component where the samples are subjected to hot rolling as mentioned before.

TABLE 3.1: Composition of 61SiCr7 spring steel

61SiCr7	***C wt.%***	***Mn wt.%***	***Si wt.%***	***Cr wt.%***
Norm-lower limit	0.57	0.70	1.60	0.20
Ovako 1-2024	0.61	0.85	1.62	0.32
Norm-upper limit	0.65	1.00	2.00	0.45

The samples which are produced in the industry results in the decarburisation layer on the surface of the components. The presence of this layer changes the surface composition of the samples by softening the surface due to low carbon content leading to reduction in the mechanical properties. The hardness values increase gradually from the surface to the core region of the components, due to the presence of the soft decarburised layer on the surface. The removal of decarburisation layer can be done by subjecting the samples to grinding process. However, the decarburisation layer is also measured in the current research using optical microscope and micro-hardness measurements which are discussed in further sections in this chapter.

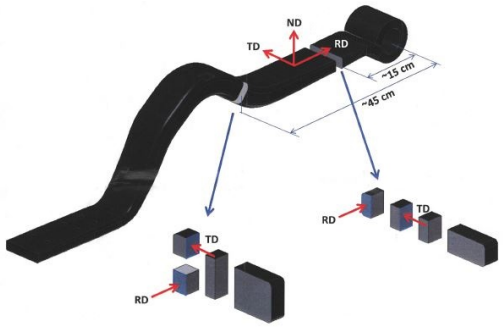

FIGURE 3.1: Sample position of 61SiCr7 spring steel

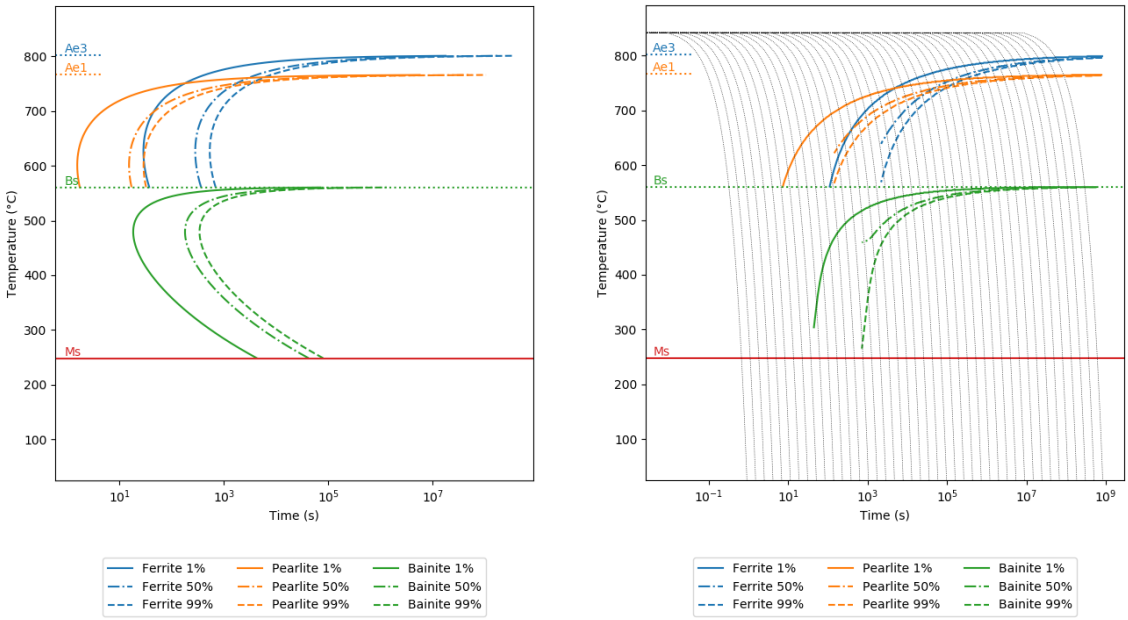

(A) (B)

FIGURE 3.2: (A) TTT diagram plotted for Fe-0.61C-1.62Si-0.85Mn-0.32Cr and (B) CCT diagram plotted for Fe-0.61C-1.62Si-0.85Mn-0.32Cr bainitic steel

Figure 3.2a illustrates the TTT diagram for the current material calculated using *Python* software. The three regions have been indicated in the respective figures representing three different phases namely, ferrite, pearlite and bainite. The horizontal lines denoting Ae_1 and Ae_3 are observed at $\sim 766^oC$ and $\sim 802^oC$ respectively. Bainitic start ($\sim 561^0C$) and martensitic start ($\sim 248^oC$) temperatures are also obtained in the figures. The value of M_s has been calculated using different models explains the temperature is more or less accurate for the current research of the material. The figures for other represented models can be observed in Appendix. Figure 3.2a represents the TTT diagram along with the cooling curves with different cooling rates from the austenitising temperature which has been plotted using *Python* software. The austenite temperature that has been represented in the plot is nearly 850^oC.

To observe the microstructural evolution of the material of 61SiCr7 steel for the research, all the samples from the transverse direction (TD), as shown in the figure 3.1, are considered. These samples helps us to identify the microscopic changes, including the decarburisation layer that occur at different heat treatment temperatures. Figure 3.3 indicates the microstructure of the steel taken from the surface, i.e., in the rolling direction of a sample after hot rolling which is

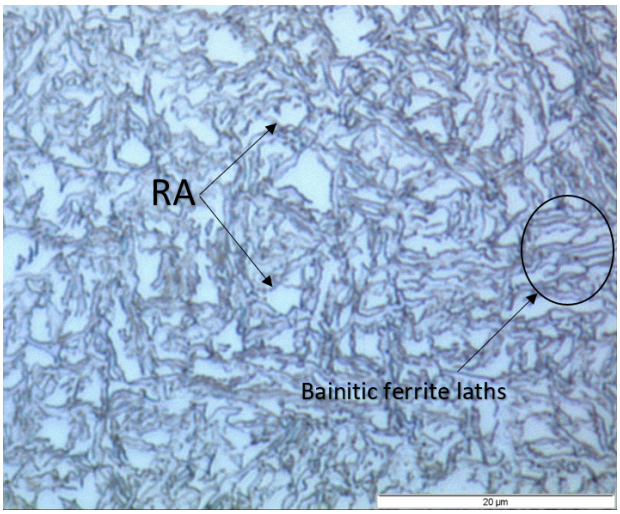

FIGURE 3.3: Microstructure of as-received material under optical microscopy illustrating mixed structures of retained austenite and bainitic ferrite laths. 2% Nital etched.

isothermally heat treated at 350^oC with a hold time of 1800 seconds. The microstructure along the rolling direction consists of different phases such as retained austenite and bainitic ferrite laths.

3.3 Heat treatments

The samples with 61SiCr7 composition were subjected to isothermal heat-treatment processes. The samples were completely austenitised and subsequently subjected to three different isothermal heat treatments where samples were categorised into different groups depending on the holding time and austempering temperature. The samples were received after the conducting all the heat treatments in the industry.

As mentioned before, there were nine different heat treatments conducted for the current research and are illustrated in the figure 3.4. Table 3.2 describes about the samples that are heat treated at the respective isothermal temperatures at respective holding times. The heat treatments has been conducted near the M_s temperature. The reason behind this is to create conditions of austempering and investigate the microstructure evolution, where usually for medium-carbon steels the microstructure of the final product is tempered martensite which is obtained by quenching and tempering. The end structure provides appropriate strength and ductility, however does not provide any fatigue resistance. Fatigue resistance is very important for heavy vehicles in spring applications in which cyclic load is constantly applied. Nevertheless, the presence of martensite in the microstructure often suffers from relatively low toughness and hydrogen embrittlement in humid and wet environmental conditions. Due to this, fatigue resistance gets affected, by decreasing significantly.

TABLE 3.2: Austempering of samples at different holding times

Austempering temperature (^oC)	**Holding time**		
	30 min	***60 min***	***120 min***
250^oC	C	A	E
300^oC	F	G	I
350^oC	J	L	M

Recently, the research on spring steels with microstructure of bainite morphology are widely in use. When bainite is formed isothermally, then the specific treatment is called austempering. During austempering, the complete austenite transformation is performed near the martensite start temperature M_s, thus avoiding non-uniform transformation, which can cause distortions and quench cracks. The samples with 61SiCr7 steel composition are austenitised above A_3 temperature for 1 hour to maintain the homogeneity and then quenched to three different temperatures i.e., 250^oC, 300^oC and 350^oC respectively. This complete transformation of austenite occurs after certain amount of holding time at respective temperatures. Therefore, the samples were held for 30 minutes, 60 minutes and 120 minutes at three different temperatures for a clear investigation.

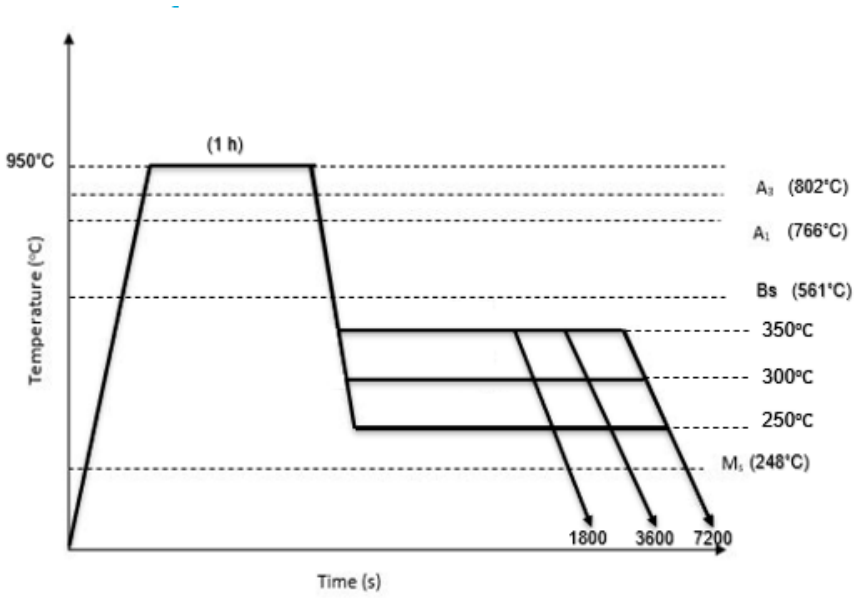

FIGURE 3.4: Schematic representation of overview of the heat treatments used in the current research

3.4 Sample preparation

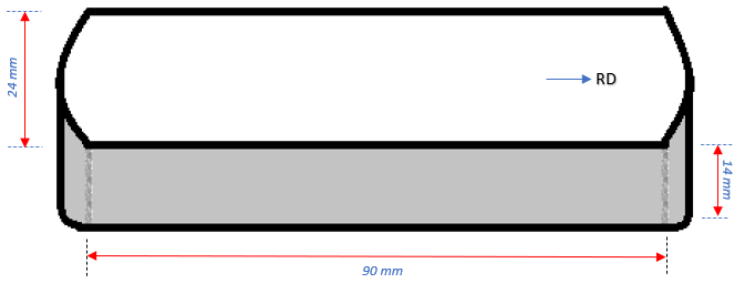

FIGURE 3.5: The schematic representation of the as-received material

As discussed in previous section, nine samples with dimensions 24mm X 90mm X 14 mm were received as shown in the figure 3.5, to examine the microstructural and mechanical property evolution. The samples were heat treated at different isothermal temperatures and holding times and later were cut at three different regions. The three regions of the each sample were

utilized for magnetisation, optical microscopy and micro-hardness measurements as shown in the figure 3.6, for further investigation. The specimens that are used for optical microscope examination are also utilized for the micro-hardness measurements to obtain a clear insight on decarburized layer which will be discussed further in detail in following sections. All the samples in transverse direction are subjected to characterization techniques after proper polishing for better understanding in the surface as well as core region of steel.

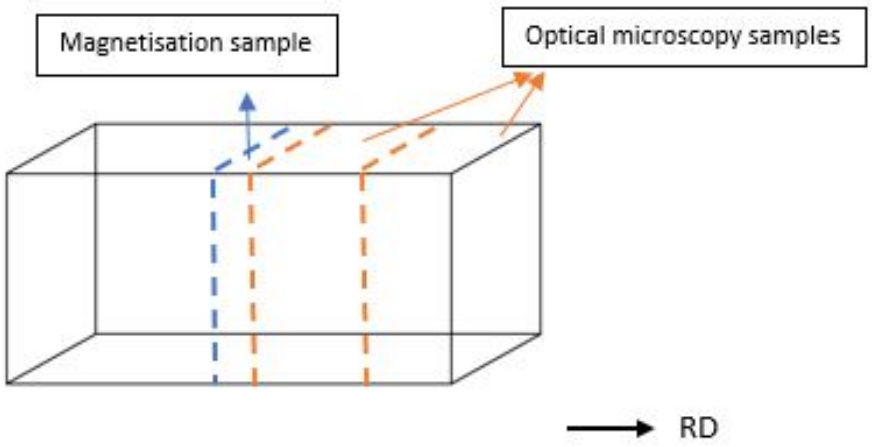

FIGURE 3.6: The schematic representation of specimens used for optical and magnetisation techniques from all samples

3.5 Metallographic technique

To process for further investigation, the as-received samples were subjected to various metallographic techniques. Before the analysis of the behaviour of the steel, the sample were subjected to techniques like cutting, mounting and polishing. The as received samples were initially subjected to cutting process for obtaining the respective specimens for different characterisation techniques. As shown in the figure 3.7, using Discotom-6 cut-off machine, the specimens for optical microscopy, magnetisation technique and micro-hardness measurements are prepared.

FIGURE 3.7: Cutt-off machine

Discotom-6 is a high performance cutting machine which can be operated automatically or manually making it suitable for over a wide range of applications. It contains a cut-off wheel with a hole diameter of 30 mm and over a 250 mm outside diameter. The speed at which the wheel can rotate is approximately 2850 rev/min [38]. A coolant system is also arranged on exactly on the top of the cut-off wheel blade which can be used to eliminate the heating burns on the cutting surface of the sample. This cooling system is a re-circulation cooling system with a volume capacity of 50 liters.

(A) (B)

FIGURE 3.8: (A) Hot mounting press and (B) Sample mounted with conductive thermoplastic resin

Subsequently, after the completion of the cutting process, the specimens are prepared. Later the samples are embedded in hard plastic mounts (figure 3.8b) using hot mounting process as shown in the figure 3.8a for grinding, polishing and further investigations. LaboPress-3 hot mounting press consisting of three variable step-wise cycles such as pressure, heating and cooling cycles has been used to prepare the samples which can reduce the sample damage during the grinding process. The device is arranged with low energy consuming electro-hydraulic mounting unit [39] where the heating temperature is $150^{o}C$ and pressure applied in $25kN$. For hot mounting, different types of thermoplastics resins can be used, where conductive resin was used to prepare the specimens in the current research. The samples were later grinded with non-adhesive SiC sanding papers from P80 (coarse grained) to P4000 (very fine grained) as shown in the table 3.3, then subjected to polishing technique using Nap cloth and Mol cloth with 3μ and 1μ diamond pastes as shown in the table 3.4 respectively, before subjecting the samples to optical microscopy and micro-hardness measurements. The diamond polishing paste is mixed with water soluble oil which can be used to observe a superfine mirror finish on the polished surface of the sample. The grinding and polishing machines are shown in the figures 3.9a and 3.9b respectively, which are equipped with water tap and drain outlet.

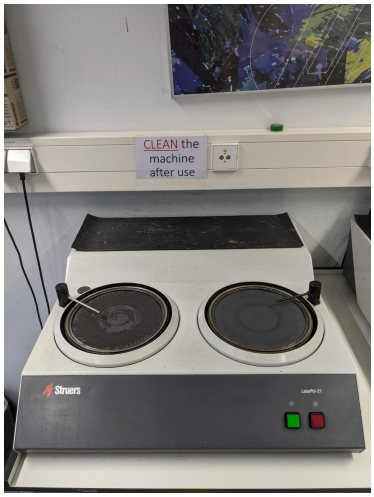

(A)

(B)

FIGURE 3.9: (A) Grinding machine (B) Polishing machine

TABLE 3.3: Sample preparation with respect to the grinding process (from right to left)

Grinding material	Time in seconds (approx)
SiC - P80	50
SiC - P180	60
SiC - P320	200
SiC - P800	200
SiC - P1200	200
SiC - P2000	250
SiC - P4000	250

TABLE 3.4: Overview of diamond polishing process

Polishing material	*Diamond suspension (3μ)*	*Diamond suspension (1μ)*
Time in seconds (approx)	*350*	*300*

3.5.1 Optical microscopy

Optical microscope is a widely used technique to observe the surface microstructure of samples. After etching, micro constituents with different chemical potential react differently with etching agent and reveal as dark and bright regions. In this way, different microstructures with different phases can be observed. As discussed in the previous section, the samples which were hot mounted into a conductive thermosetting resin, followed by grinding and polishing processes, are now subjected to micrographic examination. Before observing the phases in an optical microscope, the samples were etched with 2% Nital solution for 7 seconds and LePera solution for 75 seconds.

Later, optical microscopy is carried out using Olympus BX60M metallurgical microscope as shown in the figure 3.10, with magnifications of 10x, 50x and 100x. The surface relief effects with larger microstructural features are studied using this process. In this study, it has been used

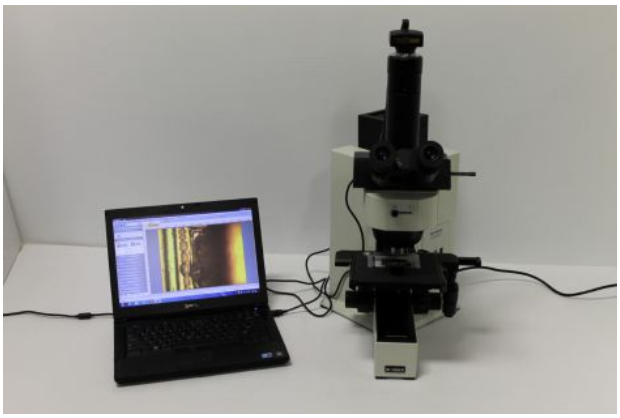

FIGURE 3.10: Optical microscope

to study the microstructural evolution, especially the effect of retained austenite at increasing isothermal temperatures and holding times. It was difficult to observe the difference between the phases like retained austenite and bainitic ferritic laths because of which, the LePera etchant with composition shown in table 3.5 was prepared and used. LePera shows bainite as dark brown or black, ferrite as brown or blue, martensite and retained austenite as white and cementite with no colour [40].

TABLE 3.5: Etchants used with respect to subjected time

Etchant	Composition	Time in seconds
Nital	99% ethanol (100 ml) + 65% Nitric acid (10 ml)	7-8
LePera	1% $Na_2S_2O_5$ in distilled water (50 ml) + 4% picric acid in ethanol (50 ml)	75-80

For a clear observation of microscopic structures, The Keyence VHX-5000 digital microscope, as shown in the figure 3.11 has been used. Keyence allows any surface to be observed with utmost focus with its depth composition. It can also switch from lower magnification (20x) to higher magnification (2500x) with ease. Keyence can also produce 3D images with high resolution images.

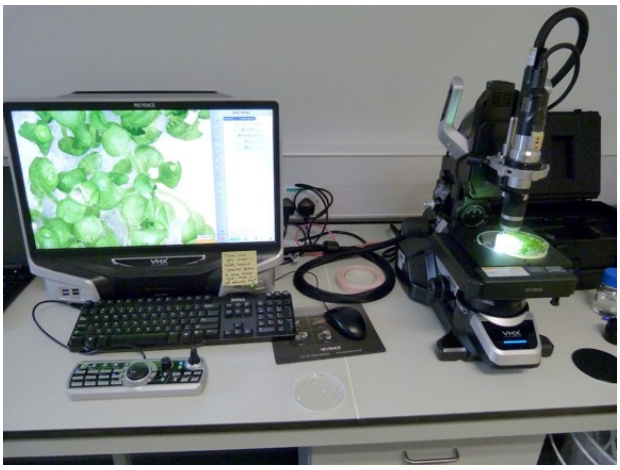

FIGURE 3.11: Keyence digital microscope

3.6 Magnetisation

Magnetic methods such as thermo-magnetic measurement analysis are widely used in metallurgical studies [41]. A Vibrating Sample Magnetometer (VSM) as shown in the figure 3.12 has been used to measure the magnetic behaviour such as saturation magnetisation of the material in the current research. According to the literature, the VSM works on the principle of Faraday's laws of induction which states that the changing the magnetic field to produce an electric field. When a sample is placed within the uniform magnetic field and subjected to mechanical vibration, magnetic flux gets affected. This induces a voltage in the coils which is directly proportional to the magnetic moment of the sample.

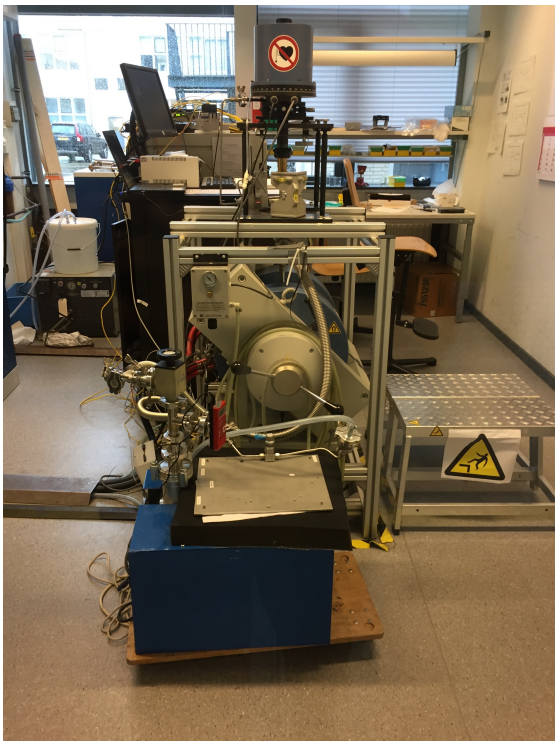

FIGURE 3.12: Magnetisation instrument

A VSM works when constant magnetic field is applied to the sample where it aligns all the magnetic domains in the direction of the applied field. In magnetisation measurements, the saturation magnetisation is derived from hysteresis loop curve. The magnetic loop or hysteresis curve is represented as the relation between magnetisation force (H) verses magnetic flux density (B). The loop begins at an initial point wherein all the magnetic dipole moments are randomly disoriented (paramagnetism). When magnetisation field is applied to the sample material, all the magnetic domains which are disoriented will start to align in the direction of applied magnetic field (as discussed previously) where magnetic flux no longer increases, following up to the saturation point. By observing the saturation in the magnetization curves, the saturation magnetization is determined, which is linearly related to the volume fraction of retained austenite. When applied magnetisation force is reduced back to zero, some amount of magnetization remains. This point is known as the retentivity (B_s). In order to remove this remained magnetization, a coercive magnetizing force is applied in the reverse direction. The point in which there is no longer a magnetic flux (B = 0) due to the cancellation of dipole moments acting in opposite directions is known as the coercivity point (H_c). As the magnetisation force increase in to negative value, the negative saturation is achieved. The same process continues and a loop is formed with an equal and opposite retentivity (-B_s) and coercivity point (-H_c) unto its saturation magnetisation is obtained. The figure 3.13 illustrates the example hysteresis loop of a medium carbon steel.

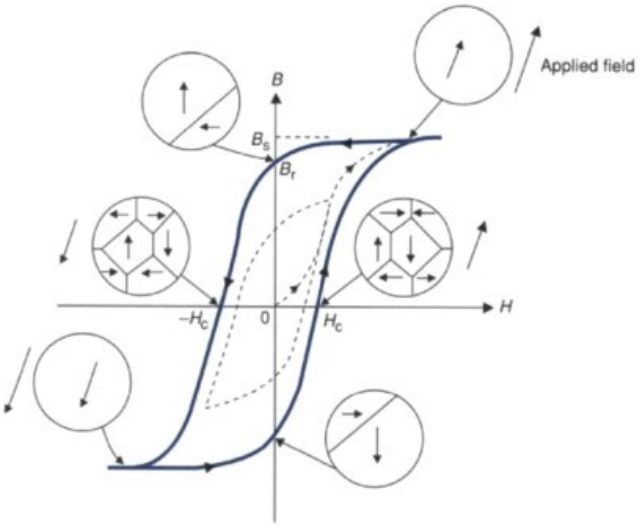

FIGURE 3.13: The schematic representation of B-H hysteresis curve in ferromagnetic material

As mentioned before, the saturation magnetisation of the sample containing austenite can be determined by the hysteresis curve. In current research, the retained austenite volume fraction can be calculated by a comparison of the saturation magnetisation values in the austenite-containing sample and saturation magnetisation of ferrite. In current research, magnetisation technique requires samples with dimensions of 3mm X 2.5mm (approximately) with 60-100 mg weight. For these kind of samples with very less heat tolerance, Struers Minitom (as shown in the figure 3.14) is used to cut the magnetisation sample from the main sample. It is also known as precision cut-off machine with low speed. A diamond cutting wheel is placed at the center of the apparatus revolves through the water container acting as a coolant system. A movable specimen holder arm is used to hold the specimen. Two weights are attached to the specimen holder at both ends where one weight balances the specimen holder with the specimen and the other weight is used to apply precised cutting pressure. During the process, the arm is subjected towards the cutting wheel using pressure from the arranged weights and produces the desired samples.

FIGURE 3.14: Magnetisation sample preparation

3.7 Micro-hardness Vickers measurements

Hardness is a characteristic material property defined as the resistance to indentation and it is determined by measuring the permanent indentation depth. Using Vickers hardness testing, also know as micro-hardness, samples are tested where a diamond indenter is forced into the material surface with a static load, leaving an impression in the form of a pyramid with a square base and opposite faces with an angle of $136^{O}C$ subjected perpendicular to the surface of the material, with certain amount of load. The most accurate hardness values are obtained from an applied load, measured using diagonal length.

FIGURE 3.15: Durascan70 micro-hardness testing machine

Micro-hardness Vickers tests were done on heat-treated samples as a measurement of their strength. The micro hardness measurements for the current research were done in the samples which were polished until 1 m and etched with LePera solution. Several measurements (∼8) were done in Struers Durascan70 micro-hardness tester, as shown in the figure 3.15. In hardness testing methods, Durascan70 is a hardness tester with a combination of complete weight system which measures hardness from micro to macro ranges i.e., from 0.01 to 10 kg with a single device. In current research, a series of measured micro-hardness readings of all the samples are calculated with *ecos Workflow* software. The diamond indenter makes an indent from which the diagonal distance (d) can be calculated and used in the equation 3.3 to find the Vickers hardness along with the value of force applied on the sample is conducted in the background of this automated programmed software. An example of indentation is shown in figure 3.16 along with the lines to measure the dimensions of the indent. The load used in this study for all the samples is 0.05 kg.

$$HV = \frac{2Fsin\frac{136^o}{2}}{d^2} \tag{3.1}$$

$$HV = 1.854\frac{F}{d^2} \tag{3.2}$$

Therefore,

$$HV = \frac{F}{A} \tag{3.3}$$

where,

$$A \approx \frac{d^2}{1.854} \tag{3.4}$$

In which, HV is Vickers hardness F is the applied force in kgf, A is the area of indentation in mm^2 and d is the distance between the opposite edges of the indents in mm.

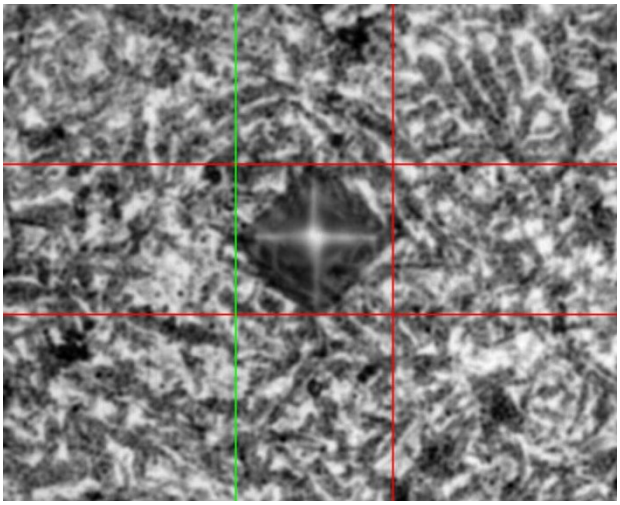

FIGURE 3.16: The diamond indenter on the sample and the horizontal and vertical lines representing the measurement of the size of the indent

Chapter 4

Results and discussion

4.1 Overview

This chapter deals with the results and discussion with respect to optical microscopy, magnetisation technique and micro-hardness measurements. The effects of retained austenite and silicon on the kinetics of bainitic transformation based on thermodynamic calculations will also be discussed in detail in this chapter.

4.2 Thermodynamic evaluation of 61SiCr7 spring steel

In this section, further details on microstructure evolution of potential constituents in the current steel as a function of temperature under equilibrium condition Using Thermo-Calc software with TCFE10 steel database and limiting the stable phases to austenite and ferrite. Figure 4.1 represents the calculation of evolution of phase fractions present. Based on the figure, at temperatures 250^oC, 300^oC and 350^oC, despite the addition of 1.62 wt.% of Si, the solidification process of the steel is conducted with the precipitation of cementite, along with BCC (ferrite) phase. The α phase decreases with increasing temperature. Figure 4.1 confirms that, under equilibrium, the maximum content of FCC (austenite) phase occurs only at relatively high temperatures i.e., from approximately 800^oC. At lower temperatures, different types of cementite are present. The carbides observed at these temperatures are chromium carbides (obtained using Thermo-Calc software).

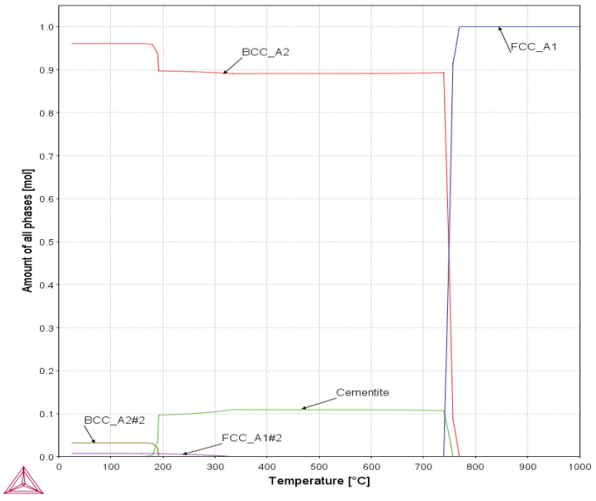

FIGURE 4.1: Evolution of fraction of phases of the studied steel calculated using Thermocalc® software

TABLE 4.1: Characteristic temperatures of three compositions using Thermo-Calc

61SiCr7	Temperatures (^oC)		
	A_3	A_1	M_s
Norm-lower limit	781	740	296
Ovako 1-2024 (current)	769	739	267
Norm-Upper limit	766	744	235

Table 4.1 represents the characteristic temperatures such as A_3, A_1 and M_S are measured using Thermo-calc software. This results that as the composition limit increases A_3 (from 781^oC to 766^oC) and M_S (297^oC to 235^oC) temperatures drops. However, the A_1 temperature varies depending on the composition of the steel.

4.2.1 Analysis of isothermal heat-treatment at 350^oC

The isothermal treatment at 350^oC was designed to investigate and understand the mechanism of bainitic transformation. Before the heat-treatment, the steel sample was rapidly cooled from austenitization temperature i.e., from 850^oC to 350^oC. In order to understand the microstructural aspects and mechanism of bainitic formation, isothermal holding times such as, 30, 60 and 120 minutes at this particular austempering temperature has also been simulated, as shown in the figure 4.2a. The figure also represents Ae_3 (801^oC), Ae_1 (766^oC), B_S (560^oC) and M_S (248^oC) temperatures. During this process, as shown in the figure 4.2b, the the amount of bainite starts to increase and the amount of austenite decreases gradually with increasing holding time. It can also be observed that the bainite reaches maximum and remains constant from 2400 seconds, representing a complete bainite formation for the steel. The characteristic temperatures obtained using Python software shows a difference of 20^oC that of the temperatures obtained using Thermo-Calc software (Table 4.1).

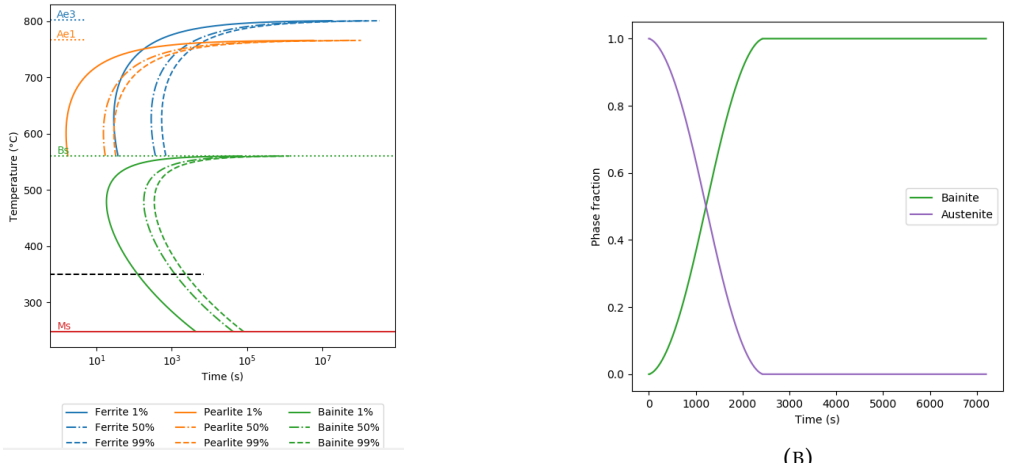

(A) (B)

FIGURE 4.2: (A) TTT diagram at 350^oC for 120 minutes and (B) Phase fractions

4.2.2 Analysis of isothermal heat-treatment at 300^oC

In this section, the microstructural evolution of the steel sample at austempering temperature 300^oC of two important phases are focused. Figure 4.3a represents the isothermal heat treatment of the steel cooled rapidly from austenitizing temperature, held for 120 minutes. This figure

represents the relative positions of the isothermal heat treatments on the time-temperature-transformation (TTT) diagram. It is clearly observed from figure 4.3b that the austenite to bainite transformation is not complete in the steel. The end microstructure consists of higher bainite phase and comparatively lesser austenite phase.

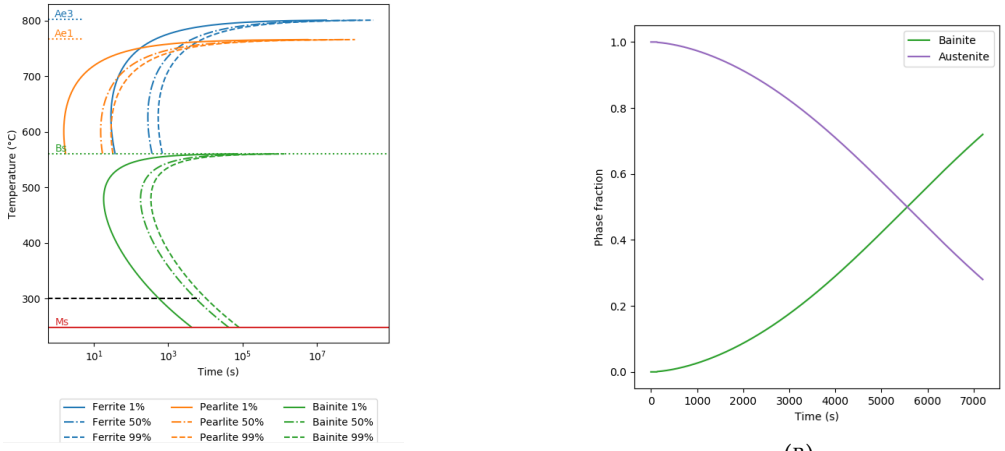

(A) (B)

FIGURE 4.3: (A) TTT diagram at 300^oC for 120 minutes and (B) Phase fractions

4.2.3 Analysis of isothermal heat-treatment at 250^oC

The calculated time-transformation-temperature diagram for the steel austempered at 250^oC is shown in the figure 4.4a. The figure also represents the isothermal hold duration of steel for 120 minutes. It can be observed form the figure that for the steel austempered at 250^oC for 120 minutes reaches the bainite start transformation line and later subsequently quenched to even lower temperatures. Figure 4.4b illustrates the fraction of phases obtained after this transformation. It can be observed that the transformation has not been started even the steel is held for 120 minutes. This results in very negligible amount of bainite formation.

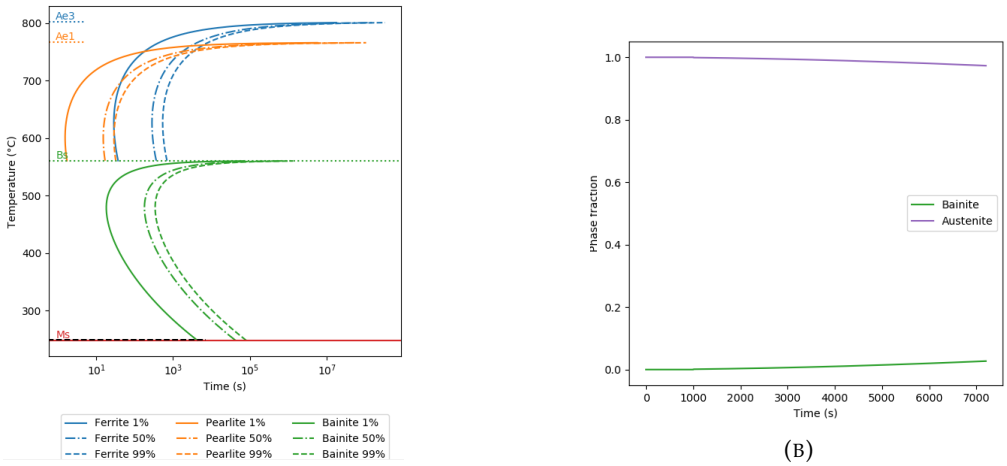

(A) (B)

FIGURE 4.4: (A) TTT diagram at 250^oC for 120 minutes and (B) Phase fractions

4.3 Optical microscope analysis

To reveal and understand the microstructural aspects of austempered 61SiCr7 spring steel, the respective samples were subjected to light metallography techniques using two different chemical reagents involving *2% Nital* and *LePera* etching solutions. Figure 4.5 represents the microstructures of heat treated samples at various austempering temperatures at different holding times using 2% Nital as etching reagent. All the microstructures are presented according to the increasing isothermal temperatures (top to bottom) at respective holding times (right to left). Bainitic ferritic laths and block shaped retained austenite are observed in the figures. It has been observed that the size and geometry of the retained austenite and inter-lath size of the bainitic ferritic sheaves varies as the isothermal temperatures and hold times are varied. Bainitic sheaves/plates appear in light brownish color, retained austenite is appear to be in white block shape in the micrographs. However, it is difficult to identify the difference between bainite and martensite.

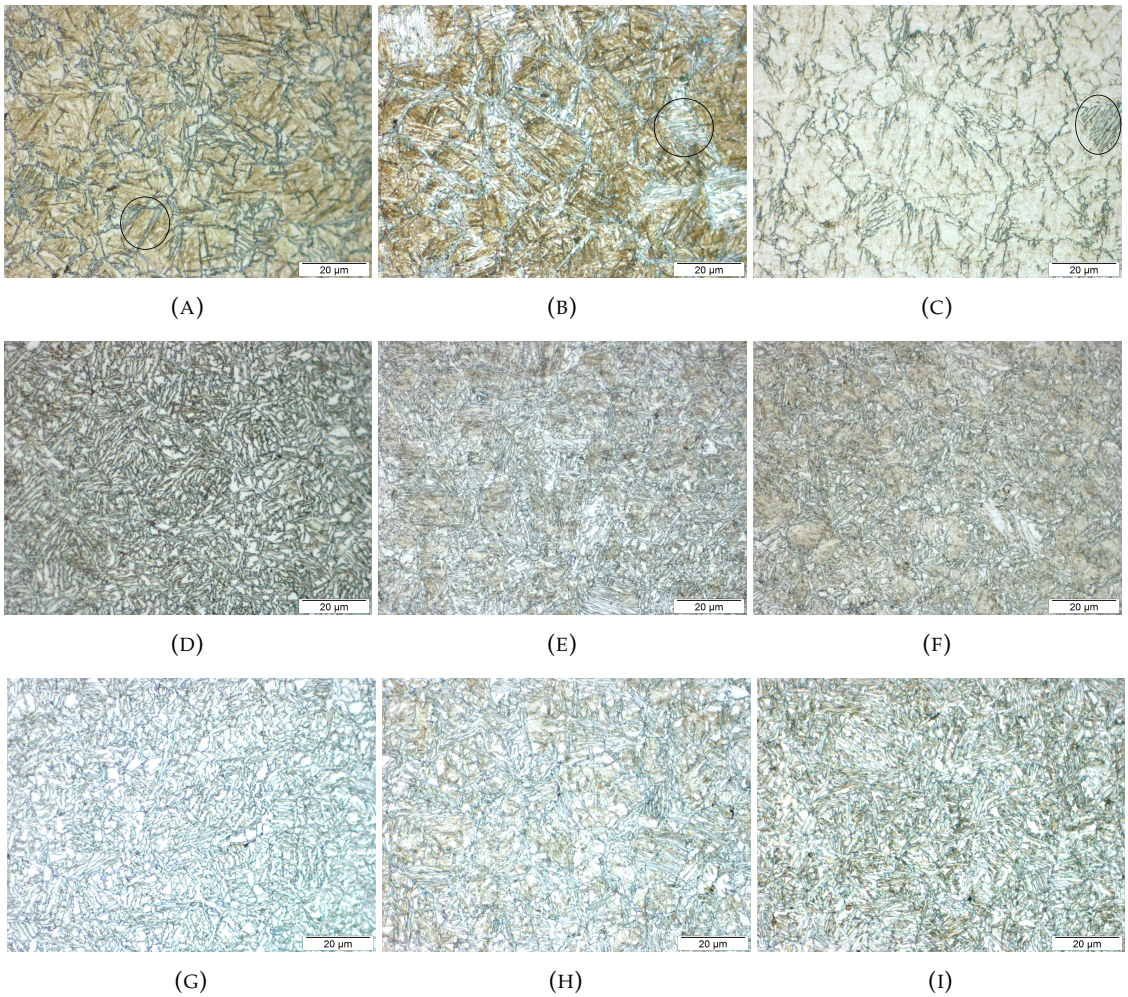

FIGURE 4.5: Optical micrographs of the samples austempered at 250^oC for (A) 30 min (B) 60 min (C) 120 min, 350^oC for (D) 30 min (E) 60 min (F) 120 min and 350^oC for (G) 30 min (H) 60 min (I) 120 min. 2% Nital etched.

In figure 4.5 (a), the steel isothermally heat treated at 250^oC after 30 minutes shows bainitic ferrite in lath morphology which are finer in compared with the figures 4.5 (b) and (c) which are subjected to isothermal heat treatment at 250^oC for 60- and 120 minutes, respectively. These regions are represented in boxes in the respective figures. Due to increase in the holding time at a specific isothermal temperature, the the thickness of the bainitic ferrite sub-units is observe to increase. However, a small amount of carbides precipitated within the acicular sub-units

and fresh martensite could also be expected to form at this temperature. These phases are difficult to identify using 2% Nital etchant. Therefore, LePera etching solution has been used to identify the phases with clear insight. It has been observed in the figure 4.6 (a)-(c) that, at higher magnification (2000x), the carbides are still difficult to identify using the micrographs. Qualitatively, this morphology gives us the characteristic feature of lower bainite. The structure which is observed in between the BF sub-unit region can be identified as RA. This can formed due to the carbon relieved into untransformed austenite during the formation of lower bainite, resulting in retained austenite in between the bainitic ferrite sub-units. However, the formation of retained austenite is observed to be less, qualitatively. And, it is difficult to identify the retained austenite for the steel austempered for 120 min.

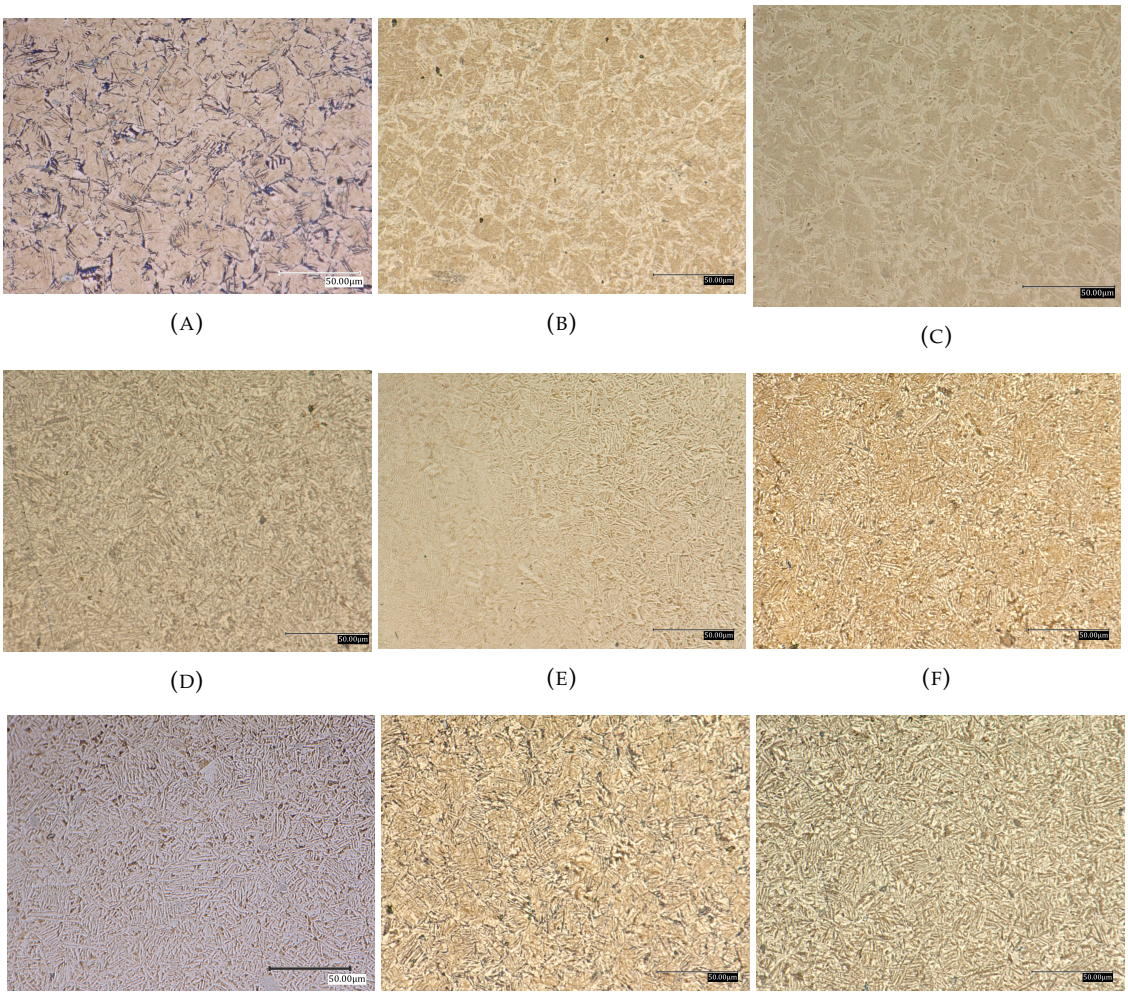

FIGURE 4.6: Optical micrographs of the samples austempered at 250^oC for (A) 30 min (B) 60 min (C) 120 min, 350^oC for (D) 30 min (E) 60 min (F) 120 min and 350^oC for (G) 30 min (H) 60 min (I) 120 min. LePera etched.

After isothermal heat treatment for 30, 60 and 120 minutes at 300^oC, the structure of the bainite slightly differs. The microstructure consists of bainitic ferrite sheaves nucleated and propagated at the austenite grain boundaries are observed to be coarser compared to with the steel austempered at 250^oC. From the figures 4.5 (d)-(e) and 4.6 (d)-(e), using both etchants, block islands of retained austenite are identified in between the bainitic ferrite laths. This indicates that there has been incomplete bainitic reaction within the holding times of 30 minutes, compared with 60 and 120 minutes.

Optical micrographs of the samples austempered at 350^oC for 30, 60 and 120 minutes are shown infigure 4.5 (g)-(h) and figure 4.6 (g)-(h) using 2% Nital and LePera etching solution, respectively. With increase in the isothermal temperature from 300^oC to 350^oC, from the micrographs, the retained austenite is observed in relatively large amounts in the form block-type, along with bainitic ferrite laths. Although, at prolonged holding time (120 minutes), bainitic ferrite with coarser morphology with smaller amounts of retained austenite are observed. After the formation of bainitic ferrite, it is observed from the micrographs that, the size of retained austenite tends to increase and on prolonged holding times from 30 to 120 minutes, the amount of retained austenite is observed to be decreased. This can be due to enough availability of time for retained austenite to transform to bainite. The morphology of bainitic ferrite in this is case is different from the morphology found at lower temperatures.

Using the micrographs of the samples isothermally heat treated at three different temperatures for three different holding times, respectively, it is qualitatively determined that with increase in both austempering temperature and holding times, the thickness of the bainitic ferrite sheaves has increased. And, with increase in austempering temperature, the amount of retained austenite has increased and with prolonged hold times, the fraction of retained austenite are observed to be decreased. A small amount of martensite must be formed during quenching from higher temperature can be observed due to the transformation of remaining austenite into martensite after quenching in post-isothermal treatment.

However, it is also difficult to identify/verify the presence of retained austenite using optical microscopy. In order to demonstrate the presence of retained austenite quantitatively, the samples are subjected to magnetisation measurement technique. The results from the measurement shows the volume fraction of retained austenite in the samples heat treated at various isothermal temperatures. This helps to understand the microstructural aspects which helps in further improving the strength and ductility in high-silicon medium carbon steels

4.4 Quantification of existing phase

It has been understood from the previous section that the presence of different phases with the help of micrographs from the isothermal heat treated samples (above M_S). The expected phases are bainitic ferrite (α) and retained austenite (γ). The presence of carbides are neglected due to the presence of high amount of silicon content in the composition of the steel. The quantification of phases, especially, retained austenite is essential in order to understand the microstructure evolution of steel. This section deals with the quantification of volume fraction of retained austenite using magnetisation measurement technique. The fraction of 100% bainite is obtained using Equation 4.1.

$$f^{\alpha} + f^{\gamma} = 1 \tag{4.1}$$

The magnetisation measurements were conducted where the applied magnetic field changed from 2 to 0 T in the steps of 0.25 T at the room temperature. The measured initial magnetisation (M) as the function of applied magnetic field (H) for different austempering temperatures and different holding times are illustrated in the figures 4.7 and 4.8. The magnetisation curves that are explained in this section by considering two plots representing the change in saturation magnetisation (M_S) at a specific austempering temperature and for specific holding time. Figure 4.7 illustrates the hysteresis curves of the steel samples austempered at 250^oC isothermally held for 30, 60 and 120 minutes. And, the figure 4.8 represents hysteresis curves of the samples isothermally held for 120 minutes at 250^oC, 300^oC and 350^oC. A detailed explanation on the

change occurring to magnetic properties due to austempering temperatures and isothermal holding times will be discussed.

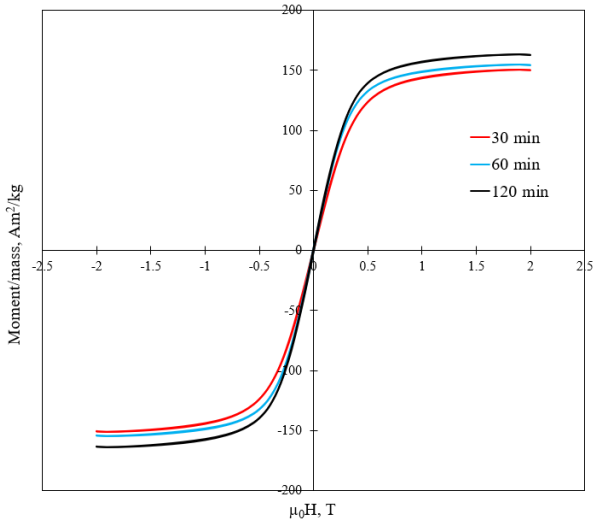

FIGURE 4.7: Magnetization (M) curves as a function of applied magnetic field (H) for steel samples austempered at 250^oC, isothermally held for 30, 60 and 120 minutes

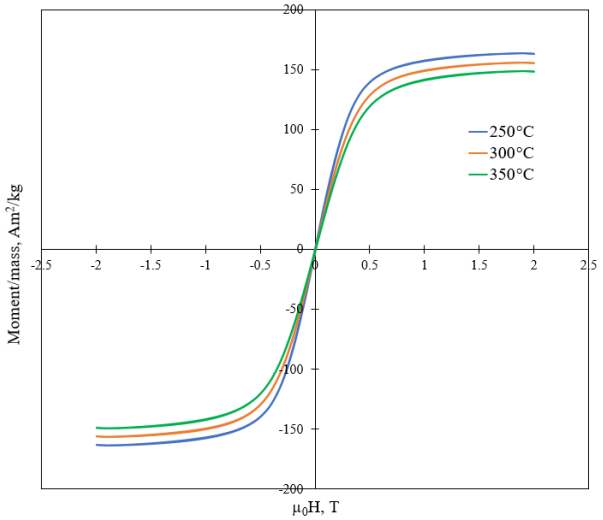

FIGURE 4.8: Magnetization (M) curves as a function of applied magnetic field (H) for steel samples isothermally held for 120 minutes at 250^oC, 300^oC and 350^oC

The saturation magnetisation increases with increasing holding time at a specific temperature (250^oC) and decreases with increasing austempering temperatures at a hold duration (120 minutes). This can be observed in figures 4.7 and 4.8.

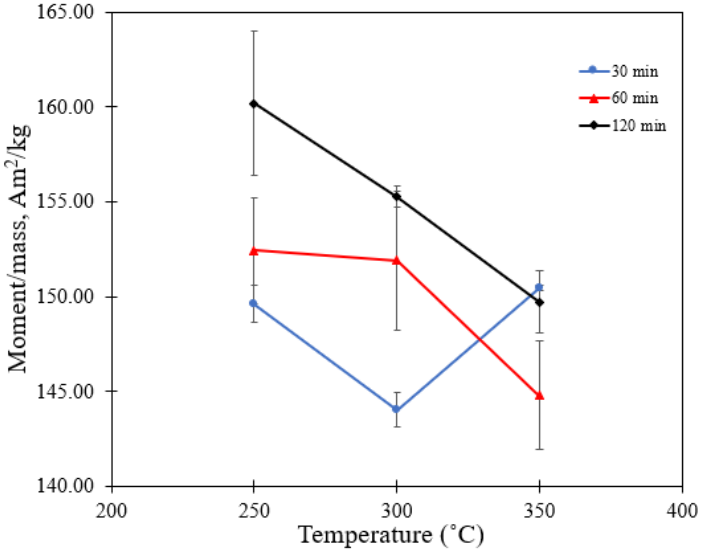

FIGURE 4.9: Magnetisation vs isothermal temperature at three different holding times

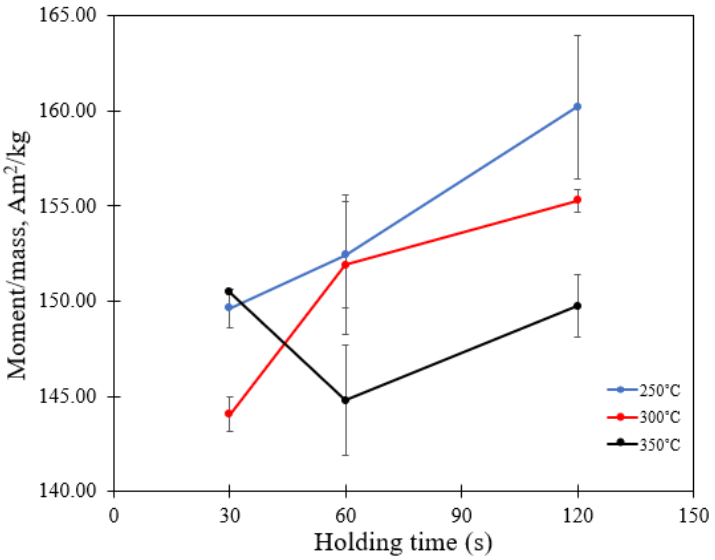

FIGURE 4.10: Magnetisation vs holding time at three different isothermal temperatures

4.4.1 Volume fraction of retained austenite from magnetisation technique

The volume of retained austenite is based on the saturation magnetisation of the samples with and without austenite phase. This is because, ferrite and cementite are ferromagnetic in nature at temperatures below the curie temperature, while austenite is paramagentic in nature. The saturation magnetisation (M_{sat}) values are obtained from the magnetisation curves and also the saturation magnetisation values of austenite-free sample ($M_{sat}(a)$) are also measured by conducting magnetisation technique. Therefore, the volume fraction of retained austenite is quantitatively obtained by following equation:

$$f^{\gamma} = 1 - \frac{M_{sat}}{M_{sat}(a)} \tag{4.2}$$

The saturation magnetisation of austenite-free sample is experimentally determined as 192.04Am^2/kg after reheating the steel sample to 650^oC for 60 minutes. The austenite-free sample has ferrite phase present in it along with small fraction of cementite. In the Equation 4.2, the fraction of cementite precipitation is assumed to be negligible after the austempering treatment of the steel samples. Because, the addition of alloying elements such as silicon reduced the formation of cementite particles significantly during the bainitic transformation. Table 4.2 represents the volume fraction of RA obtained from magnetisation curves, with not more than 2% error.

TABLE 4.2: Fraction of retained austenite with respect to austempering temperatures

Austempering temperature (^oC)	Holding time (min)					
	30	error (%)	60	error (%)	120	error (%)
250	0.2188	1	0.2042	1	0.1636	2
300	0.2480	1	0.2068	2	0.1894	1
350	0.2145	1	0.2441	1	0.2183	1

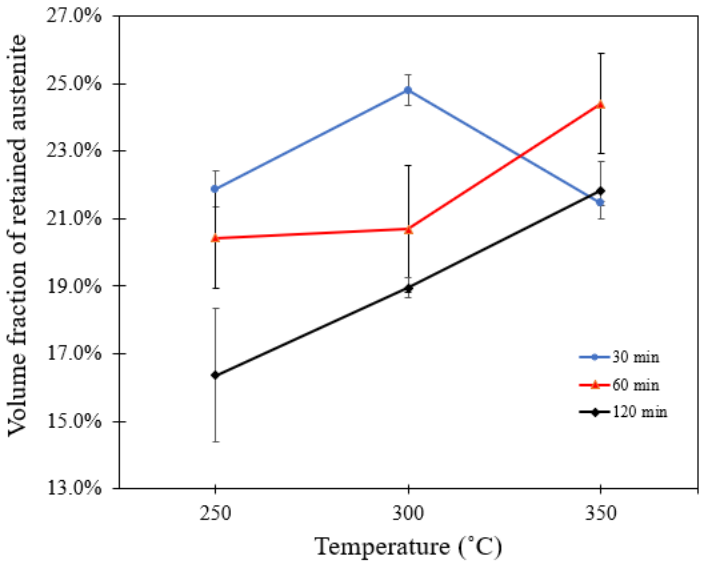

FIGURE 4.11: Volume fraction of retained austenite vs isothermal temperature at three different holding times

Quantitatively measured the volume fraction of retained austenite (f^γ) is plotted as a function of austempering temperatures and isothermal holding times, as shown in figures 4.11 and 4.12. The figure 4.11 illustrates the change in volume fraction of RA as a function of austempering temperature at 30, 60 and 120 minutes hold duration. It is observed from the figure that the RA fraction increases with increasing austempering temperature, for the steel samples isothermally held for 60 and 120 minutes. The samples isothermally held for 60 minutes shows negligible increasing trend (20.4% and 20.7%) as the austempering temperature increases from 250^oC to 300^oC, respectively. For the same sample austempered at 350^oC shows significant raise to 24.4% of the amount of RA. Similarly, the sample isothermally held for 120 minutes shows an increasing trend from 16.4% at 250^oC to 18.9% at 300^oC and later to 21.8% at 350^oC. This is due to, during the sample isothermally held for 60 minutes (short holding time compared with 120 minutes), the austenite is transformed to bainitic ferrite where the transformation is not complete. Due to which, the excess carbon from the parent austenite is retained and allows to form RA to a greater extent when compared with prolonged holding time. Although, during the prolonged holding

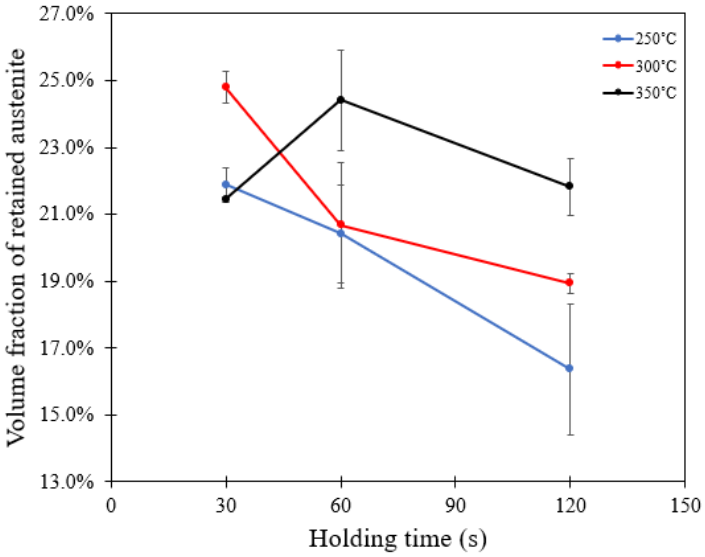

FIGURE 4.12: Volume fraction of retained austenite vs holding time at three different isothermal temperatures

duration, the carbon has sufficient amount of time to diffuse from austenite phase, leads to form more amount of bainitic ferrite and less amount of RA.

However, the steel sample isothermally held for 30 minutes, the fraction of RA initially increases with increasing austempering temperature and decreases at 350^oC. There can be two possibilities:

- Due to less availability of carbon content present in the steel sample austempered at 350^oC for such short duration of holding time, when compared with the steel sample austempered at 300^oC. Equations 4.3 and 4.4 represents the the presence of less amount of RA in the steel austempered at 350^oC, isothermally held for 30 minutes:

$$\chi^{\gamma}_{C_{350}} \ll \chi^{\gamma}_{C_{300}} \tag{4.3}$$

$$f^{B}_{350} < f^{B}_{300} \tag{4.4}$$

- It can also be explained due to the heterogeneity of carbon distribution in the austenite grains, at that specific sample. It can be assumed that the grain size of the austenite to be very large leading to the formation of bainitic ferrite to a larger extent, implying the presence of less amount of RA, at that specific sample.

It can be observed from figure 4.12 that, at each austempering temperature i.e., for 250^oC and 300^oC, the volume fraction of retained austenite decreases with increasing isothermal holding time. For 60 minutes hold duration, the fraction of RA is almost the same for the samples austempered at 250^oC and 300^oC. Although, the sample austempered at 350^oC shows a large difference of amount of RA with 24%, when compared with 250^oC. Because, the driving force of bainitic transformation is high at lower temperatures. The bainitic ferrite formed form the austenite phase is larger at 300^oC which enhances the formation of bainite in the steel.

However, the steel sample austempered at 350^oC, the fraction of RA increases initially from 21% to 24% with increasing holding time from 30 minutes to 60 minutes and later decreases to 22% with increasing duration. Generally, the bainitic ferrite formed at a specific austempering

temperature contains high carbon content. After enough amount of hold time, the excess amount of carbon present in the bainitic ferrite is rejected and leads to the formation of RA. However, with prolonged holding time at a specific austempering temperature, the amount of RA is transformed to bainitic ferrite and carbides.

4.5 Decarburized layer and its effects

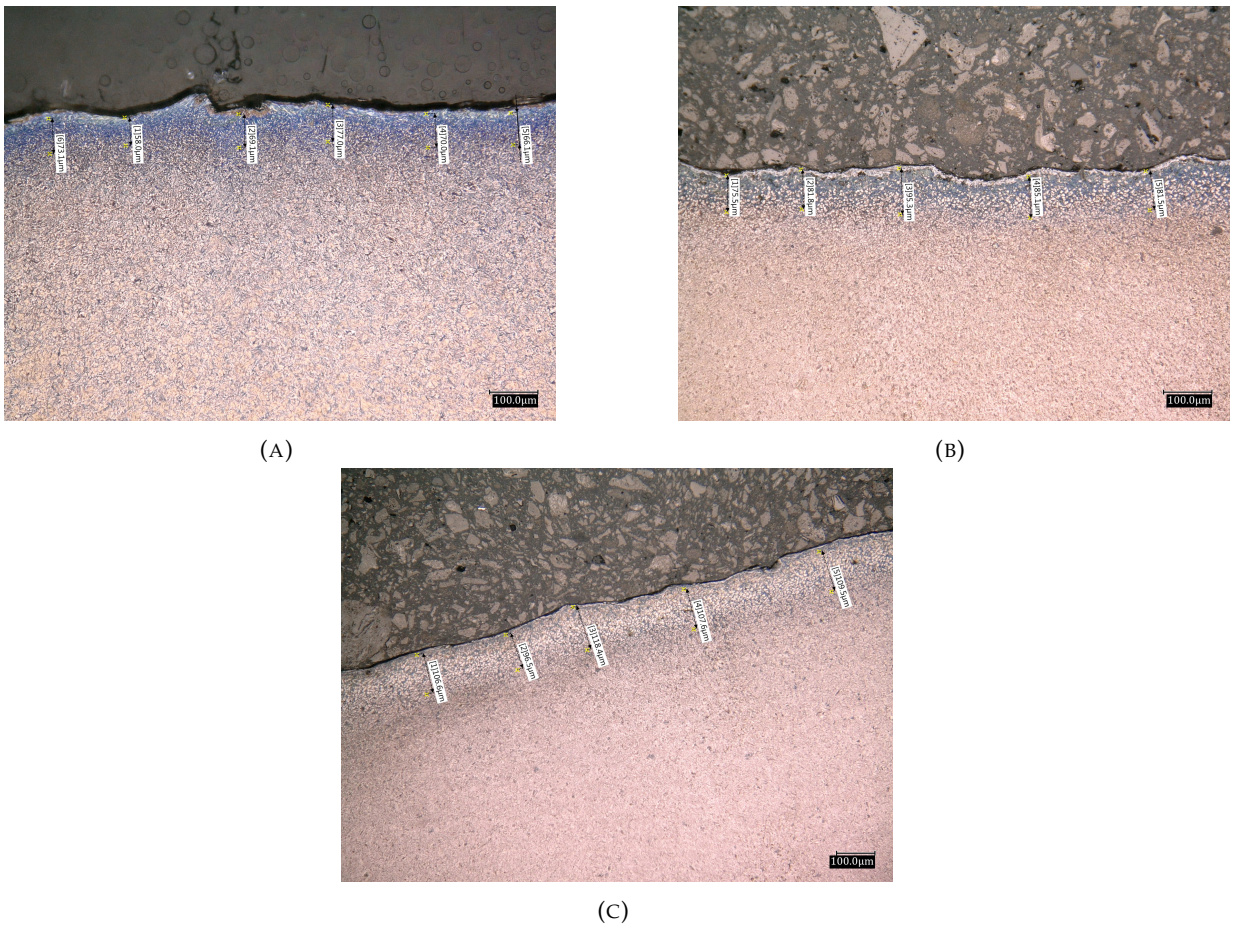

(A) (B)

(C)

FIGURE 4.13: Optical micrographs of the samples austempered at (A) 250^oC for 30 minutes, (B) 300^oC for 30 minutes and (C) 350^oC for 30 minutes

The loss of carbon in the surface region of the steel sample is known to be as decarburization. During the production process, the steel samples are subjected to furnaces to conduct isothermal heat treatments. During the process, at higher temperatures, due to the presence of high amount of oxygen, a decarburized layer on the surface is formed. At higher temperatures, the rate diffusion of carbon is very high that at prolonged isothermal heat treatment will lead to the formation of a decarburized layer. The mechanism of decarburization generally leads to the increased fraction of ferrite and reduction in the fraction of carbides, as shown in the figure 4.13. Generally, decarburized layer is measured as the sum of partial and complete decarburization [42]. Partial decarburized layer is found as an area at which the presence of carbon in a reduced state.

During optical microscopy evaluation, the depth of decarburized layer is determined on the basis of change in contrasts of the different phases. Figure 4.13 represents the depth of the decarburized layers of the samples austempered at 250^oC, 300^oC and 350^oC, isothermally held for 30 minutes. The depths of the layer has been noted from the optical microscopy measurements for the samples austempered at 250^oC is measured $66.1\mu m$, 300^oC with $81.5\mu m$ and 350^oC with $109.5\mu m$. It has been understood that the depth of decarburization obtained in the surface region of the specific steel samples increases with increase in austempering temperature, at a specific isothermal hold duration. Decarburization layer helps to study the mechanical properties of the steel which is correlated with the microstructural aspects for further investigations.

4.6 Micro-hardness measurements

It can be understood that hardness of the steel results in better strength. Therefore, the mechanical property of any steel is generally characterized by measuring the hardness of the steel. In this section, the results from the micro-hardness measurement supports the microstructural evolution at different austempering temperatures and isothermal holding times. Figure 4.14 is optical micro-graph of the sample austempered at 350^oC for 30 minutes hold duration. Three specific sets of 8 hardness values are measured across the cross-section of the steel, starting from the sample surface, i.e., from decarburized layer to the bulk region of the steel.

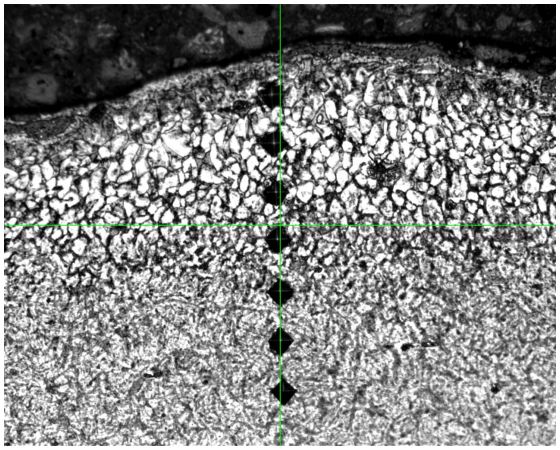

FIGURE 4.14: Micro-hardness indents measured from the decarburization layer to the bulk region

Figure 4.15 represents the micro-hardness values of the austempered at 250^oC, 300^oC and 350^oC at 30, 60 and 120 minutes. The hardness values are determined along the depth distance of the steel samples. In these plots, the hardness increases with increasing depth distance. This is due to the presence of decarburized layer present on the surface of the sample, resulting in lower hardness values. After a depth of $0.07mm$ (approximately), the decarburized layer ends and increase in hardness is observed. In figure 4.15 (a), (b) and (c), at depth of $0.25mm$ from the surface, a plateau in the curve indicating the saturation period is observed. This implies that the hardness remains constant in the bulk region of the sample. Although, the hardness values increases with increasing depth until $0.2mm$. The depth distance of the sample from $0.07mm$ to $0.2mm$, the reason behind the increase in hardness is due to effect of decarburized layer on the adjacent regions, leading to an increasing trend.

The samples used for quantitative calculation of the fraction of RA are taken from the bulk region. Therefore, the hardness values from the bulk region of the steel samples are the area of interest. From figure 4.15 (a), the sample austempered at 250^oC shows higher hardness values when in compared with the samples austempered at 300^oC and 350^oC, which are isothermally held for 30 minutes. Similarly, for the samples with hold duration of 60 minutes, austempered at 250^oC shows higher hardness values, as shown in (b). However, as shown in (c), the sample austempered at 300^oC shows higher hardness values from $0.01mm$ to $0.22mm$. Later, in the process of reaching bulk region, the sample austempered at 250^oC shows higher hardness values, i.e., from $0.25mm$ to $0.35mm$. The scattering of hardness values observed in the figure 4.15 (a) and (c) are due to high segregation of alloying elements or in-homogeneously distribution of alloying elements gives higher hardness values.

To analyse the hardness measurements as a function of isothermal temperatures with a clear insight, figure 4.16 is plotted. From the figure 4.16, the hardness values decreases with increasing austempering temperatures for the samples isothermally held for 30, 60 and 120 minutes. The samples isothermally held for 120 minutes, shows a decreasing trend from $478HV$ to $466HV$ and later to $449HV$ for the samples austempered at 250^oC, 300^oC 350^oC respectively. Similarly, for the samples isothermally held for 60 minutes, also shows decreases from $462HV$ to $456HV$ and later to $441HV$ as the austempering temperatures increases from at 250^oC, 300^oC to 350^oC. However, sample isothermally held for 30 minutes initially decreases from $446HV$ to $425HV$ with increasing austempering temperature from 250^oC to 300^oC and later increases to $443HV$ for the sample austempered at 350^oC. The decrease in hardness is due to the amount of RA present in the steel.

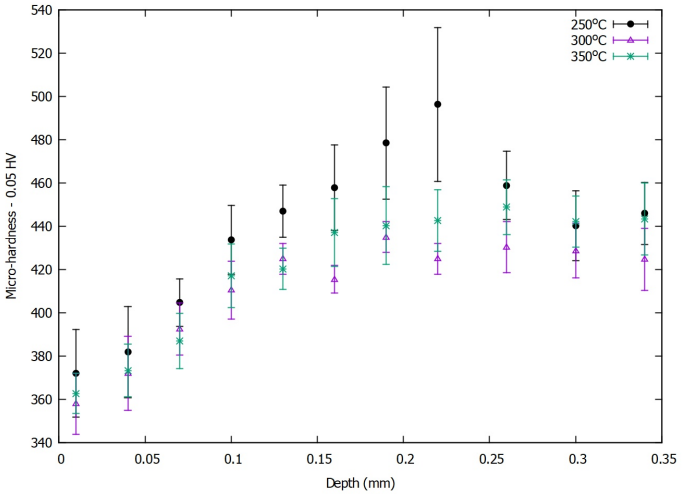

(A)

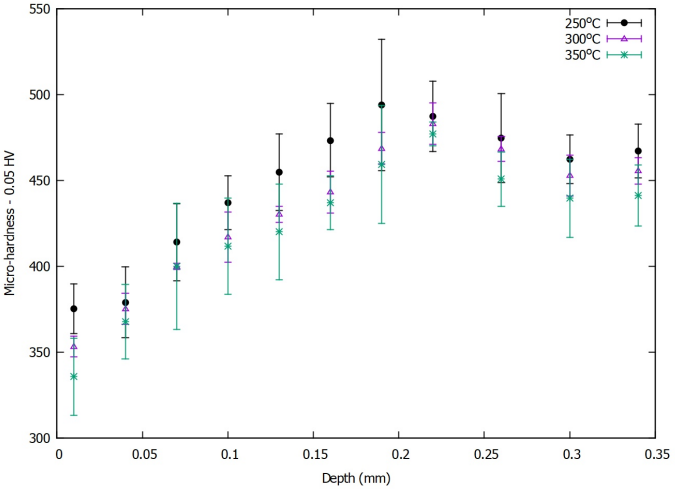

(B)

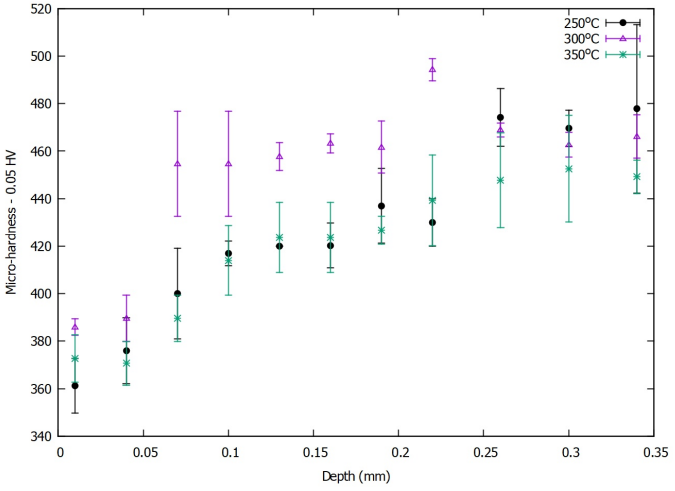

(C)

FIGURE 4.15: Micro-hardness values with respect to sample depth distance at holding time (A) 30 minutes, (B) 60 minutes and (C) 120 minutes for three different austempering temperatures

During isothermal transformation, with increase in bainitic ferrite where the excess carbon moves to the austenite present in the adjacent regions, becomes more soluble. This results in the formation of RA. Correlating with figure 4.11, it can be analysed that decreasing trend in hardness is a result of increasing trend of amount of RA present in the steel, with increase in austempering temperature. As the temperature increases, at prolonged duration of 120 minutes results in the decomposition of RA to bainite and carbides to a greater extent when compared with the samples isothermally held for 30 and 60 minutes, which results in higher hardness values. However, at relatively higher temperature, i.e., at 350^oC isothermally held for 30 minutes, the amount of RA present is less when compared with the sample austempered at 300^oC. This results in increasing trend in hardness measurement as the austempering temperature increases from 300^oC to 350^oC. This variation in the results of the amount of RA and micro-hardness measurements as a function of austempering temperatures at different hold duration are in consistent with the results obtained from magnetisation technique (section 4.4.1).

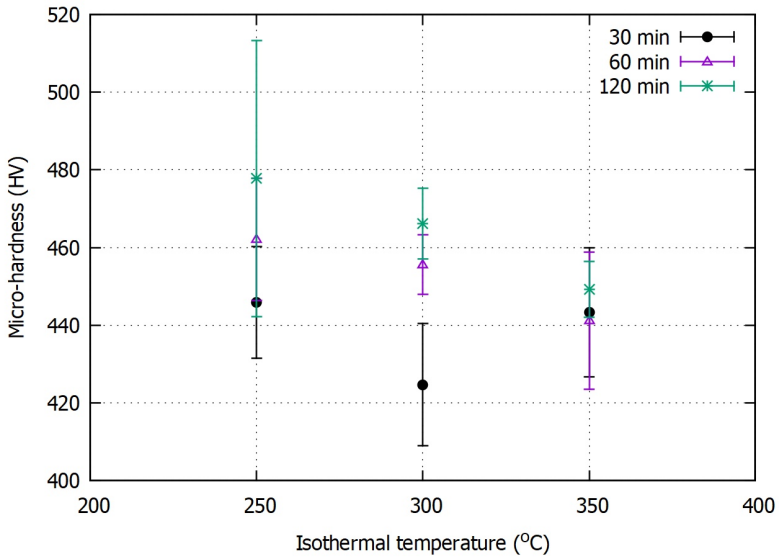

FIGURE 4.16: Micro-hardness as the function of isothermal temperatures (^oC)

4.7 Kinetics of austenite to bainite transformation

Thermodynamic calculations were performed using Thermo-Calc software and the TCFE10 thermodynamic database. In Figure 4.17 the phase diagram of 61SiCr7 spring steel, is presented. The two phase region of austenite and ferrite for the isothermal process is evident and denoted as $\alpha+\gamma$.

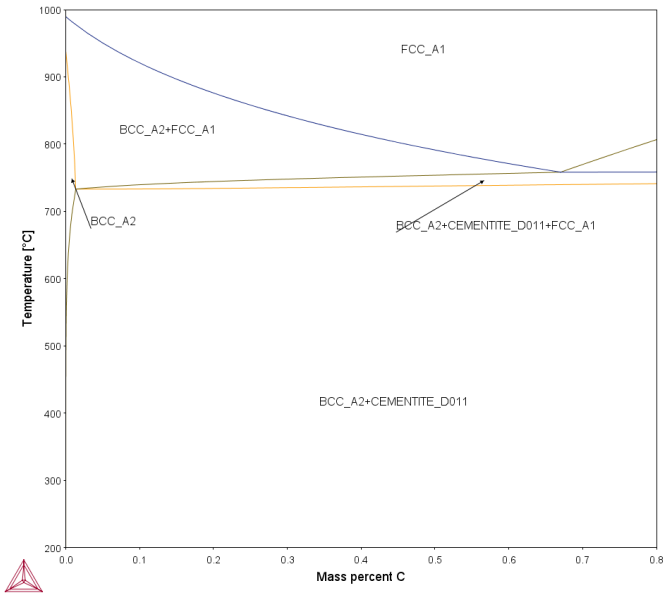

FIGURE 4.17: The phase diagram of Fe-0.61C-1.62Si-0.85Mn-0.32Cr steel in para-equilibrium condition

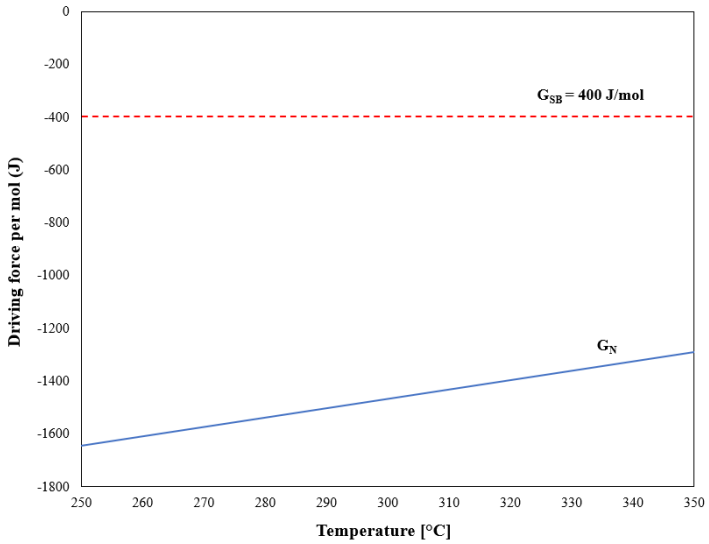

FIGURE 4.18: Composition free energy versus austempering temperature for diffusion-less mechanism. G_N is the universal nucleation function

From figure 4.18 it can be understood that the driving force for nucleation of bainitic ferrite at 250^oC, 300^oC and 350^oC is calculated for the steel, using the empirical equation 2.2. The calculations were performed using Thermo-Calc software. In the temperature range of bainite, the *universal nucleation function* appears well below the required energy of bainite (equal to $400 J/mol$). This can be implied by relating to equation 2.4 that these conditions ensures both the

conditions, firstly, the chemical free energy change exceeds the energy of bainite, and secondly that nucleation takes place.

4.7.1 Isothermal transformation kinetics using JMAK equation

An important aim of material science is to understand the fraction of phase transformed during the transformation at a specific amount of time, with respect to nucleation and growth aspects. In this study, the mechanism of the transformation of austenite to bainitic ferrite (V_B) and carbides (V_C) during prolonged isothermal holding times has been mathematically computed. This is gained by measuring fraction of retained austenite (V_{RA}) through Equation 4.5,

$$V_B + V_C = 1 - V_{RA} \tag{4.5}$$

Since fraction of carbide transformation has been neglected, the mechanism of the transformation of austenite to bainitic ferrite (V_B) during given isothermal holding time is derived using Equation 4.6,

$$V_B = 1 - V_{RA} \tag{4.6}$$

The fraction transformed to retained austenite is measured using magnetisation technique, as mentioned in section 4.4.1. As, the transformation is in solid-state, the mechanism of isothermal transformation of austenite to bainite is computed by a JMAK relation (Equation 4.7), as mentioned in section 2.7.1:

$$f = 1 - exp(-kt^n) \tag{4.7}$$

where, f is the transformed fraction, n is the Avrami exponent, k is the rate constant and t is the time after the transformation onset.

Rearranging the terms and applying logarithm on both sides of the equation gives:

$$ln[ln[1/(1-f)]] = nlnt + lnk \tag{4.8}$$

Equation 4.8 is a derived version of Equation 4.7 which implies the transformation behaviour of the solid phases. This equation is used to analyse the data using logarithmic plots. Figure 4.19 shows the JMAK curves at different austempering temperatures. The plot determines the decomposition rate of austenite phase at different austempering temperatures at various holding times. $ln[ln[1/(1-f)]]$ on the y-axis is a linear function with isothermal holding time (lnt) on x-axis. Slope of the resultant linear fit and y axis-intercept determines the Avrami constants, n and k, respectively.

TABLE 4.3: Avrami constants at various austempering temperatures

Austempering temperature (^oC)	**Avrami constants**	
	n	**k**
250	0.125	0.585
300	0.126	0.546
350	-0.0079	1.589

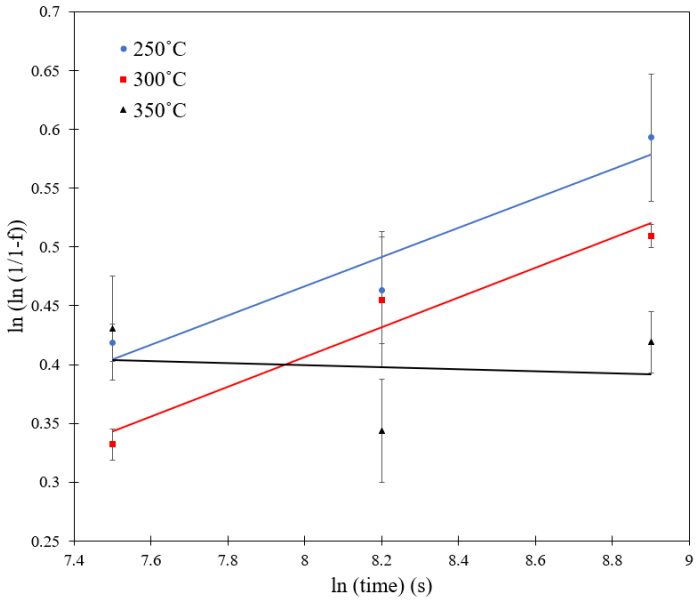

FIGURE 4.19: The rate of decomposition of austenite on isothermal holding times at different austempering temperatures

Values of Avrami constants n and k have been measured using the slope and intercepts of the straight lines fitted to the data points through linear regression analysis. Table 4.3 represents the values of n and k which corresponds to respective austempering temperature. The Avrami constant, n depends on the rate of nucleation and growth mechanisms of the solid phases. Therefore, investigating the value of n helps to understand the phase transformation at a specific austempering temperature. From table 4.3, it can be understood that, n value increases as the austempering temperature increases from 250^oC to 300^oC. However, later shows decreasing trend at 350^oC. The lower value of n at 350^oC implies that the rate of transformation of austenite to bainitic ferrite is lower, when compared with 250^oC and 300^oC. Therefore, at this particular steel sample, due to slow rate of transformation, the partition of carbon into retained austenite is also less.

In bainitic temperature range, k value is temperature dependant. It can also be seen from table 4.3 that the steel sample austempered at 350^oC shows the highest k value. This implies that the transformation from austenite to bainite at 350^oC has been completed to a larger extent, with slower transformation rate (as mentioned in the previous paragraph). This can be due to high driving force at lower temperatures, leading to activation of larger number of nucleation sites [43]. Due to which, decreasing trend in fraction of retained austenite from 300^oC to 350^oC has been observed as shown in figure 4.9 supports the observation. And, from analysing the model, it has been understood that JMAK model is not suitable for the steel sample austempered at 350^oC for 30 minutes. The n value less than 0 does not exist. The reason for observing the decreasing trend at this specific steel sample is still unknown.

4.8 Para-equilibrium

The morphological changes occurring at different austempering temperatures can be further interpreted using thermodynamics. As discussed in the section 2.7, the transformation from austenite to ferrite can be studied using the free energy diagram, as shown in the figure 2.7. The T_0 line in the diagram represents the similar free energy values of austenite and ferrite. In

the figure 4.20, Ae_1 and Ae_3 lines are represented as the composition of ferrite and austenite at equilibrium condition, respectively. However, in order to investigate the kinetics of phase transformation under para-equilibrium condition, thermodynamic calculations were performed using Thermo-Calc software with TCFE10 database. The A_3 and A_1 lines are calculated in the para-equilibrium condition at a temperature range of $200 - 400^oC$. Figure 4.20 illustrates the para-equilibrium and T_0 lines which are extrapolated to lower temperatures.

Figure 4.20 shows the T_0 line obtained by Thermocalc software. During the calculation the carbides precipitated are not neglected. T_0 temperature is a temperature at which both the phases, austenite and ferrite contains same Gibbs free energy for the steel with this specific composition. T_0 temperature also represents schematically the locus of points. The T_0 temperature is determined as the common tangent line where for which austenite and ferrite have equal free energies.

The T_0 line meets the 0.61% carbon content dotted line represented in the figure 4.20. This temperature is the limit temperature for the diffusion-less transformation of the steel. The dots on the dotted line in the figure represents the austempering temperatures at which the steel samples are heat treated to study the microstructural evolution. Consequently, the bainitic transformation must be conducted within the range of 561^oC (B_S) and 233^oC (M_S) temperatures. Although, from the previous sections, it can concluded that the steel is isothermally heat treated at temperatures 250^oC, 300^oC and 350^oC, within in the range of the bainitic transformation temperatures. When the steel is heat treated with this range, the free energy of the bainite becomes less when compared with the free energy of austenite. The entire para-equilibrium calculations are conducted considering the steel with same composition. In the bainitic transformation, during under cooling, the excess carbon is rejected into the austenite in adjacent regions. If the carbon concentration of the austenite reaches T_0 line, the process of bainitic transformation is hindered. However, the carbon concentration which transforms into carbides, its fraction is determined by the isothermal holding time and its alloy content.

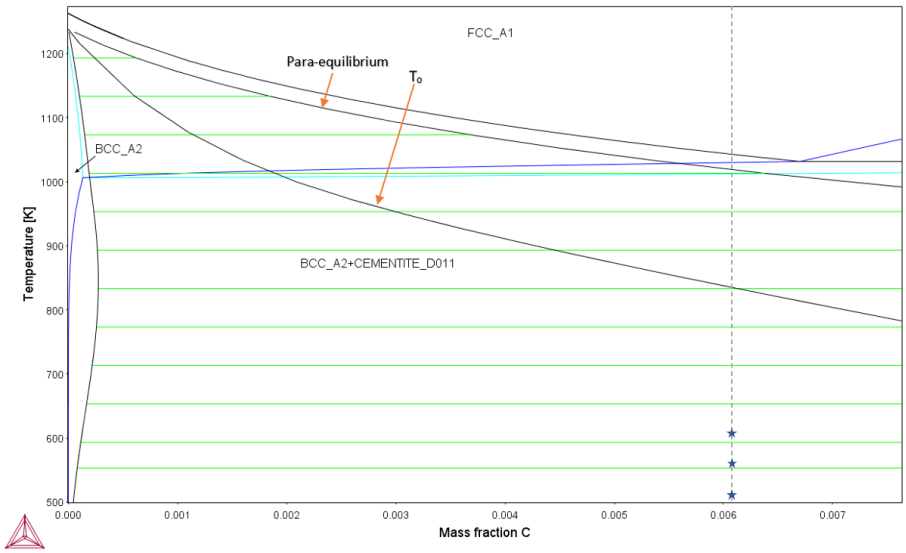

FIGURE 4.20: Calculated isothermal sections of the para-equilibrium phase diagram

4.8.1 Redistribution of carbon

In the calculation of carbon concentration in austenite, the values are arranged to calculate the super saturation of carbon in austenite, which also depends on the isothermal temperature involved in the bainitic transformation. The figure 4.21 is derived from the figure 4.20. The T_0 line extended to lower temperatures to measure the super saturation of carbon in austenite at temperatures 250^oC, 300^oC and 350^oC. The table 4.4 represents the theoretical thermodynamic results of the amount of carbon concentration present in the austenite and volume fraction of remaining austenite (RA) which is calculated using equation 4.9:

$$f_{RA} = \frac{C_{steel}}{C_{austenite}} \tag{4.9}$$

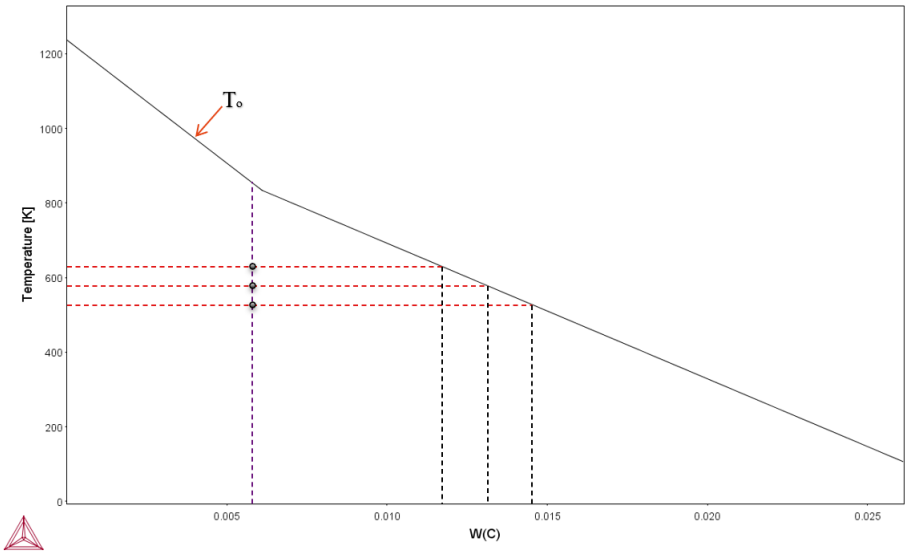

FIGURE 4.21: Calculated extrapolated T_0 line of the phase diagram under para-equilibrium condition

TABLE 4.4: Calculated carbon concentration in austenite and fraction of remaining austenite, under para-equilibrium condition

Austempering temperature (^oC)	Mass percent C (%)	Fraction of RA (%)
250	1.4	0.44
300	1.28	0.48
350	1.16	0.53

Figure 4.22 represents the formation of remaining austenite during the transformation as the function of austempering temperature, which is measured using the austenite carbon content calculated thermodynamically. This plot shows that, during the nucleation and growth of bainite, the carbon is discharged from the bainitic sub-units that forms when the parent austenite reaches T_0 composition. This leads to increase in the final fraction of remaining austenite, with increase in austempering temperature [44]. The amount of austenite formed at 250^oC, 300^oC and 350^oC are 0.44%, 0.48% and 0.53%, respectively. These theoretical thermodynamic results roughly matches with the experimental results of fraction of retained austenite formed, from section 4.4.1.

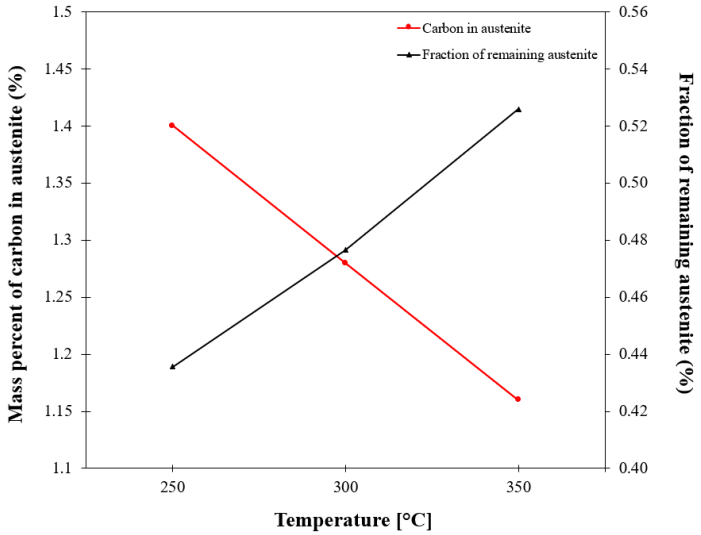

FIGURE 4.22: Calculated carbon concentration in austenite and fraction of remaining austenite as a function of austempering temperature under para-equilibrium condition, at T_0 line

From volume fraction of RA predicted using thermodynamic analysis is higher comparatively than obtained by magnetisation technique. The thermodynamic analysis theoretically determines the fraction of RA, however, by magnetisation technique, it can probe the bulk region of the steel resulting in more accurate results. Although, this study produces a better validation to the results obtained from section 4.4.1.

4.9 Effects of silicon

As discussed in the section 1.3.1, various literature has been stated the influence of silicon on the bainite formation and its hardness values. Figures 1.4a and 1.4b represents the effect of fraction of retained austenite with respect to increasing silicon content, produces a better understanding on the current research. In current research with 1.62% silicon concentration in para-equilibrium condition, during the isothermal transformation at 300^oC, at 0.61% carbon concentration, the phases present are bainitic ferrite and retained austenite. This calculation has been conducted using Thermocalc software with TCFE10 database as shown in the figure 4.23.

Figure 4.24 represents the influence of silicon on the fraction of cementite particles in the para-equilibrium condition, as a function of temperature. The plot is plotted using Thermocalc software, which results, as the temperature increases, the fraction of cementite gradually increases and later remains constant from 338^oC. It has been also observed that for the steel with silicon concentration of 1.6 wt.% and 1.62 wt.% shows negligible change in the fraction of cementite. However, when the concentration of silicon increases to 2.0 wt.%, the amount of volume fraction of cementite formation in the steel decreases.

In para-equilibrium conditions, it is difficult to observe the formation of cementite due to lack of driving of force for the precipitation. The formation of para-equilibrium cementite is only observed when the silicon is partitioned during the transformation process, which evidently takes prolonged duration. From the figure, it has been understood that the results obtained from the thermodynamic calculations of Thermocalc software shows that the Si concentration present

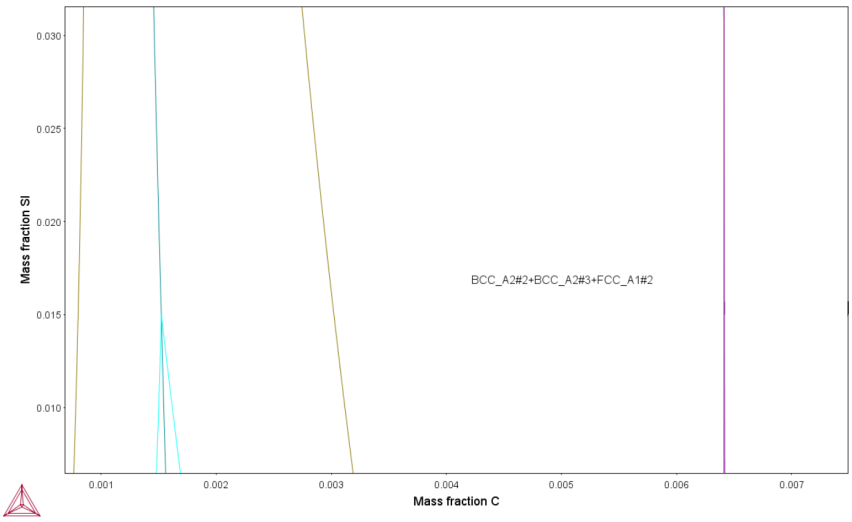

FIGURE 4.23: The phase fraction of silicon with respect to the fraction of carbon, in para-equilibrium condition

in the steel is not sufficient to prevent the formation of cementite during the transformation. This can be due to the presence of high amount of silicon present in the supersaturated austenite. This reduces the carbon concentration in remaining austenite, leading to the formation of bainitic ferrite. Due to which the reduction in the volume fraction of RA has been observed. This supports the information obtained from section 4.4.1.

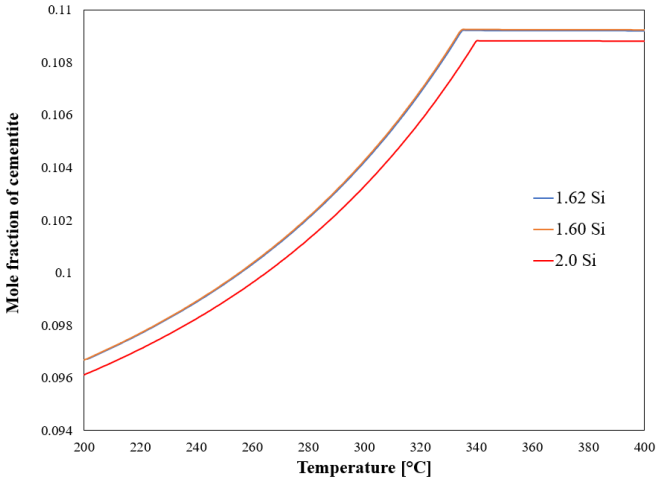

FIGURE 4.24: Phase fraction of cementite in para-equilibrium with austenite as a function of temperature

Chapter 5

Conclusion and Recommendation

5.1 Conclusions

The study on 61SiCr7 high silicon spring steel isothermally heat-treated at three different temperatures and holding times produced the following results:

- The steel samples heat-treated isothermally at 250^oC, 300^oC and 350^oC contained bainitic ferrite and retained austenite phases. The austenite decomposes into bainitic ferrite, retained austenite and carbide. Due to the presence of 1.62% Si in the composition, the formation of carbides is prevented and considered to be negligible. When the steel is subjected to longer holding times, the retained austenite is observed to be decomposed into bainitic ferrite during the transformation. It was found that the retained austenite appears as block- and film shaped in the inter-lath region of the bainitic ferrite. However, it is difficult to quantify the size and type of retained austenite using optical microscopy and magnetisation technique.
- During isothermal holding at the austempering temperatures resulted in the formation of bainite even at short holding times, for example the steel austempered at 350^oC for 30 minutes. However, for this sample, the amount of retained austenite formed is less than the retained austenite formed during heat treatment at 300^oC. This can be due to the in-homogeneous distribution of the carbon or the due to the presence of high amount of carbon in the steel sample austempered at 300^oC.
- The steel austempered at 250^oC exhibited better mechanical properties such as micro-hardness. This is due to the presence of less fraction of retained austenite.
- The micro-hardness show decrement with the increase in isothermal temperatures and prolonged holding times. The steel subjected to isothermal heat treatment at 250^oC and 300^oC for 60 and 120 minutes holding times shows decrement in micro-hardness. However, the micro-hardness of the steel austempered at 350^oC held for 30 minutes increases with temperature due to incomplete transformation into bainitic ferrite, allowing less carbon to accommodate retained austenite.
- JMAK model conducted works better for the steel austempered at lower and intermediate temperatures (250^oC and 300^oC) in compared with the steel austempered higher temperature (350^oC). This indicates that the JMAK model is not suitable for the steel austempered at 350^oC. Avrami exponent obtained through this model concludes that the nucleation of bainite is observed to be one-dimensional (1-D).
- The thermodynamic study under para-equilibrium condition and with T_0-temperature line, it concludes that the fraction of remaining austenite increases with increasing temperature, which supports with experimentally measured retained austenite.

- The effect of silicon on the bainite transformation kinetics has been thermodynamically studied. Although, the presence of silicon has a significant effect on cementite, the thermodynamic study concludes that the concentration of silicon (1.62%) present in the steel is not sufficient to prevent the formation of cementite. This leads to reduction in the carbon concentration austenite, which also leads to increase in the formation of bainitic ferrite resulting in reduction of fraction of RA.

5.2 Recommendations

The recommendations which can assist in further investigations for current research of study are:

- The volume of bainite formed during the transformation at lower isothermal temperatures (250^oC) is unclear with optical microscopy technique and could be observed with better magnification using SEM and TEM. This could help to understand the nucleation and growth mechanism of the phase and also helps to compare the bainite morphology to the morphology observed at higher isothermal temperatures.
- The fraction of retained austenite formed in the steel austempered at 250^oC, 300^oC and 350^oC at 30, 60 and 120 isothermal holding times, respectively, could be quantitatively measured by conducting Electron Back-scattered Diffraction (EBSD) analysis. which gives a better understanding on the performance of the steel.
- The effect of Si concentration on the kinetics of bainitic transformation is still unclear. Thus study on the different steels with varying Si concentrations could be beneficial in understanding the mechanism of cementite.
- Using an alternative model to study the kinetics of bainitic transformation at higher temperatures could result in better understanding on the concept.

Appendix A

Appendix

A.1 Time-transformation-temperature (TTT) diagram validation

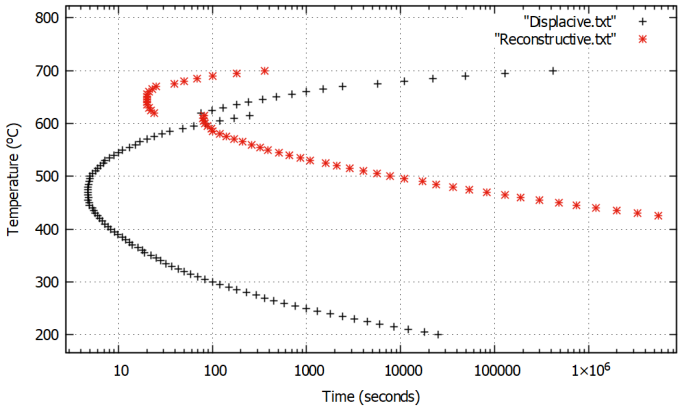

FIGURE A.1: Calculated TTT diagram with two C-curves using MUCG46 software

A Time-transformation-temperature diagram has been plotted using MUCG46 software in order to validate the characteristic temperatures. Figure A.1 illustrating the two C-curves representing reconstructive and displacive mechanisms of the steel. The table A.1 gives the information on the bainitic and martensitic start temperatures which can be used to validate with the results obtained from Thermo-Calc and Python softwares.

TABLE A.1: Characteristic temperatures obtained from Bhadeshia software (MUCG46)

Bainite start temperature	$429^{o}C$
Martensite start temperature	$253^{o}C$

A.2 Composition of different types cementite at different austempering temperatures

TABLE A.2: Chemical composition of carbides at 250^oC

250^oC	**Chemical composition**				
	Cr	**C**	**Mn**	**Fe**	**Si**
BCC_A2#1	4.62716E-6	1.94273E-8	0.00010	0.98218	0.01772
Cementite_D011	0.01207	0.06706	0.09975	0.82112	4.70445E-13
FCC_A1#2	0.76071	0.18703	0.04938	0.00288	2.29269E-12

TABLE A.3: Chemical composition of carbides at 300^oC

300^oC	**Chemical composition**				
	Cr	**C**	**Mn**	**Fe**	**Si**
BCC_A2#1	0.00002	9.03685E-8	0.00021	0.98200	0.0177
Cementite_D011	0.02329	0.06712	0.09528	0.81432	4.70800E-13
FCC_A1#2	0.77739	0.18711	0.03035	0.00515	8.92052E-12

TABLE A.4: Chemical composition of carbides at 350^oC

350^oC	**Chemical composition**				
	Cr	**C**	**Mn**	**Fe**	**Si**
BCC_A2#1	0.00006	3.27355E-7	0.00041	0.98171	0.01782
Cementite_D011	0.03460	0.06716	0.08951	0.80872	4.71149E-13
FCC_A1#2	-	-	-	-	-

Bibliography

[1] AC Baviskar, VG Bhamre, and SS Sarode. Design and analysis of a leaf spring for automobile suspension system: a review. *International Journal of Emerging Technology and Advanced Engineering*, 3(6):407–410, 2013.

[2] TB Hilditch, T de Souza, and PD Hodgson. Properties and automotive applications of advanced high-strength steels (ahss). In *Welding and Joining of Advanced High Strength Steels (AHSS)*, pages 9–28. Elsevier, 2015.

[3] Jornsen Reimpell, Helmut Stoll, and Jurgen Betzler. *The automotive chassis: engineering principles*. Elsevier, 2001.

[4] Critical raw materials - eu. [Online; accessed 03-May-2020].

[5] Trailing arm. [Online; accessed 03-May-2020].

[6] T Ko and SA Cottrell. The formation of bainite. *Journal of the Iron and Steel Institute*, 172(3):307, 1952.

[7] HKDH Bhadeshia and DV Edmonds. The mechanism of bainite formation in steels. *Acta Metallurgica*, 28(9):1265–1273, 1980.

[8] Yuki Toji, Hiroshi Matsuda, and Dierk Raabe. Effect of si on the acceleration of bainite transformation by pre-existing martensite. *Acta Materialia*, 116:250–262, 2016.

[9] Thomas Sourmail and Véronique Smanio. Low temperature kinetics of bainite formation in high carbon steels. *Acta Materialia*, 61(7):2639–2648, 2013.

[10] B Karbakhsh Ravari and M Nili Ahmadabadi. Influence of alloying elements on the bainitic transformation of ductile iron. In *Key Engineering Materials*, volume 457, pages 175–180. Trans Tech Publ, 2011.

[11] E Kozeschnik and HKDH Bhadeshia. Influence of silicon on cementite precipitation in steels. *Materials Science and Technology*, 24(3):343–347, 2008.

[12] Changle Zhang, Hanguang Fu, Jian Lin, and Yongping Lei. The effect of silicon on microstructure and wear resistance in bainitic steel. *Transactions of the Indian Institute of Metals*, 72(5):1231–1244, 2019.

[13] Zhang Changle, Fu Hanguang, Ma Shengqiang, Yi Dawei, Lin Jian, Xing Zhenguo, and Lei Yongping. Effect of mn content on microstructure and properties of wear-resistant bainitic steel. *Materials Research Express*, 6(8):086581, 2019.

[14] Kangying Zhu, Hao Chen, Jean-Philippe Masse, Olivier Bouaziz, and Gabriel Gachet. The effect of prior ferrite formation on bainite and martensite transformation kinetics in advanced high-strength steels. *Acta materialia*, 61(16):6025–6036, 2013.

[15] George Krauss. Deformation and fracture in martensitic carbon steels tempered at low temperatures. *Metallurgical and Materials Transactions B*, 32(2):205–221, 2001.

[16] Zhi-Gang Yang and Hong-Sheng Fang. An overview on bainite formation in steels. *Current Opinion in Solid State and Materials Science*, 9(6):277–286, 2005.

[17] Sylvain Dépinoy, Caroline Toffolon-Masclet, Stéphane Urvoy, Justine Roubaud, Bernard Marini, François Roch, Ernst Kozeschnik, and Anne-Françoise Gourgues-Lorenzon. Carbide precipitation in 2.25 cr-1 mo bainitic steel: effect of heating and isothermal tempering conditions. *Metallurgical and Materials Transactions A*, 48(5):2164–2178, 2017.

[18] William D Callister Jr and David G Rethwisch. *Callister's Materials Science and Engineering*. John Wiley & Sons, 2020.

[19] Harshad Kumar Dharamshi Hansraj Bhadeshia and JW Christian. Bainite in steels. *Metallurgical transactions A*, 21(3):767–797, 1990.

[20] M Takahashi and HKDH Bhadeshia. Model for transition from upper to lower bainite. *Materials Science and Technology*, 6(7):592–603, 1990.

[21] Reynolds WT, HI Aaronson, G Spanos, et al. A summary of the present diffusionist views on bainite. *Materials Transactions, JIM*, 32(8):737–746, 1991.

[22] David A Porter and Kenneth E Easterling. *Phase transformations in metals and alloys (revised reprint)*. CRC press, 2009.

[23] Seong Hoon Kim, Kwan-Ho Kim, Chul-Min Bae, Jae Sang Lee, and Dong-Woo Suh. Microstructure and mechanical properties of austempered medium-carbon spring steel. *Metals and Materials International*, 24(4):693–701, 2018.

[24] HKDH Bhadeshia. Bainite in steels–transformation, microstructure and properties. *Institute of Materials, 1 Carlton House Terrace, London, SW 1 Y 5 DB, UK, 2001. 454*, 2001.

[25] HKDH Bhadeshia. Diffusional and displacive transformations. *Scripta metallurgica*, 21(8):1017–1022, 1987.

[26] VC Igwemezie and PC Agu. Development of bainitic steels for engineering applications. *Int. J. Eng. Res. Tech*, 2:2698–2711, 2014.

[27] Quanshun Luo, Matthew Kitchen, and Shahriar Abubakri. Effect of austempering time on the microstructure and carbon partitioning of ultrahigh strength steel 56nicrmov7. *Metals*, 7(7):258, 2017.

[28] George F Vander Voort. *Atlas of time-temperature diagrams for irons and steels*. ASM international, 1991.

[29] J Kang, FC Zhang, XW Yang, B Lv, and KM Wu. Effect of tempering on the microstructure and mechanical properties of a medium carbon bainitic steel. *Materials Science and Engineering: A*, 686:150–159, 2017.

[30] A Varshney, S Sangal, AK Pramanick, and K Mondal. On the extent of transformation of austenite to bainitic ferrite and carbide during austempering of high si steel for prolonged duration and its effect on mechanical properties. *Materials Science and Engineering: A*, 793:139764, 2020.

[31] Binggang Liu, Wei Li, Xianwen Lu, Xiaoshuai Jia, and Xuejun Jin. The effect of retained austenite stability on impact-abrasion wear resistance in carbide-free bainitic steels. *Wear*, 428:127–136, 2019.

[32] SB Singh. Mechanisms of bainite transformation in steels. In *Phase Transformations in Steels*, pages 385–416. Elsevier, 2012.

[33] RF Hehemann, KR Kinsman, and HI Aaronson. A debate on the bainite reaction. *Metallurgical Transactions*, 3(5):1077–1094, 1972.

[34] Carlos Capdevila, Juan Cornide, Kouji Tanaka, K Nakanishi, and E Urones-Garrote. Kinetic transition during ferrite growth in fe-c-mn medium carbon steel. *Metallurgical and Materials Transactions A*, 42(12):3719, 2011.

[35] Yogev Amran, Alexander Katsman, Peter Schaaf, and Menachem Bamberger. Influence of copper addition and temperature on the kinetics of austempering in ductile iron. *Metallurgical and Materials Transactions B*, 41(5):1052–1058, 2010.

[36] HKDH Bhadeshia. The nature, mechanism and properties of strong bainite. In *Proceedings of the 1st International Symposium on Steel Science (IS3–2007), The Iron and Steel Institute of Japan*, volume 94. Citeseer, 2007.

[37] Francisca G Caballero, Carlos Capdevila, Carlos Garcia-Mateo, and Carlos García de Andrés. Evaluation of displacive models for bainite transformation kinetics in steels. 2006.

[38] Discotom-6 cut-off machine. [Online; accessed 03-May-2020].

[39] Struers labopress-3 hot mounting press. [Online; accessed 03-Aug-2020].

[40] Ersoy ERİŞİR, Serap GÜMÜŞ, and Oğuz Gürkan BİLİR. Microstructural characterization of medium carbon dual phase steels after intermediate quenching. *Proceedings of Metal*, pages 15–17, 2013.

[41] Lie Zhao, NH Van Dijk, E Brück, J Sietsma, and S Van der Zwaag. Magnetic and x-ray diffraction measurements for the determination of retained austenite in trip steels. *Materials Science and Engineering: A*, 313(1-2):145–152, 2001.

[42] B Edenhofer, D Joritz, M Rink, and K Voges. Carburizing of steels. In *Thermochemical Surface Engineering of Steels*, pages 485–553. Elsevier, 2015.

[43] Babak Shahriari, Reza Vafaei, Ehsan Mohammad Sharifi, and Khosro Farmanesh. Continuous cooling transformation behavior and the kinetics of bainite formation in a bainitic–martensitic steel. *International Journal of Materials Research*, 108(9):715–724, 2017.

[44] Daniel Gaude-Fugarolas and Pascal J Jacques. A new physical model for the kinetics of the bainite transformation. *ISIJ international*, 46(5):712–717, 2006.